CHAPTER II
LITERATURE REVIEW

2.1 Previous Technology: Semiconductor Solar Cells

In a traditional solid-state semiconductor with p-n junction, a solar cell is made from two doped crystals, one doped with n-type impurities (n-type semiconductor), which has extra free electrons, and the other doped with p-type impurities (p-type semiconductor), which is to increase free holes. The band structures of differently-doped semiconductors are shown in Figure 2.1. When placed in contact, some of electrons in the n-type portion will flow across the boundary into the p-type to "fill in" the hole until the Fermi levels of the two materials are equal as shown in Figure 2.2. The result is a region at the interface, the p-n junction, where the bent bands represent a built-in electric field over what is referred to as the depletion region (www.dur.ac.uk/~dph0www5/solar.html.; Grätzel, 2001). In silicon, this transfer of electrons produces a potential barrier of about 0.6 to 0.7 V (en.wikipedia.org/wiki/Dye-ensitized_solar_cell#cite_note-10).

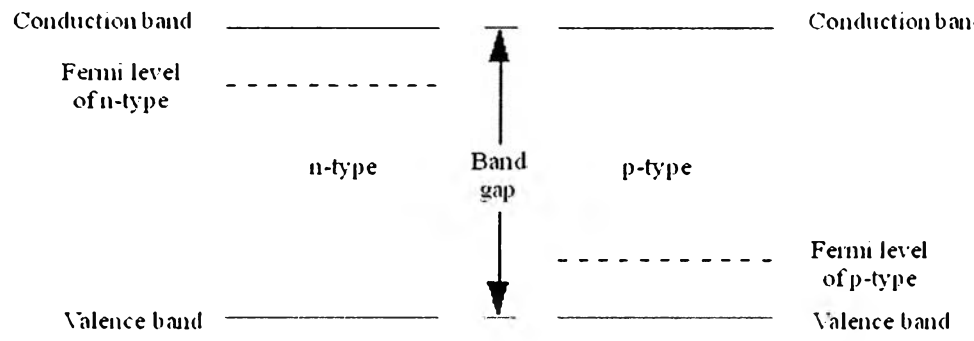

Figure 2.1 Band structures of differently-doped semiconductors (www.dur.ac.uk/ ~ dph0www5/solar.html.).

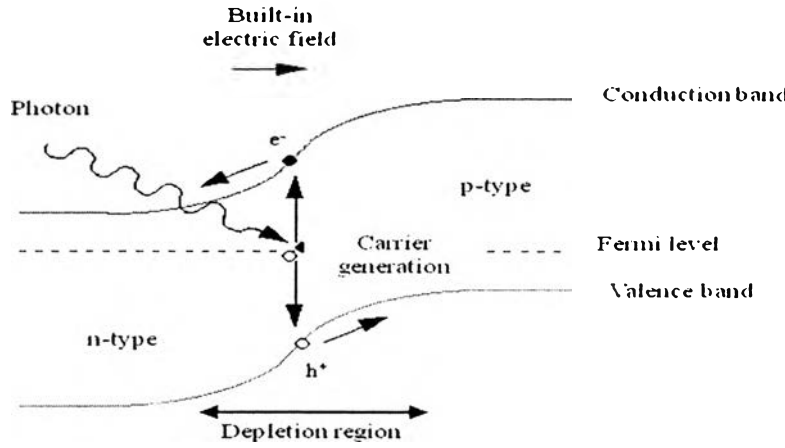

Figure 2.2 Principle of photovoltaic device (www.dur.ac.uk/~dph0www5/solar.html.).

When placed in the sun, photons of the sunlight strike the bound electrons in the n-type side of the semiconductor, giving them more energy to push an electron out of the valence band into the conduction band where electrons are free to move around the silicon. When a forward bias is placed across the cell as a whole, these electrons will flow out of the n-type side into the p-type side, lose energy while moving through the external circuit, and then back into the n-type material where they can once again re-combine with the valence-band hole they left behind. In this way, sunlight creates an electrical current (www.dur.ac.uk/~dph0www5/solar.html.).

2.2 Solar Cell Efficiency Factors

2.2.1 Thermodynamic Efficiency Limit

Photons with energy below the band gap of the absorber material cannot generate a hole-electron pair, and so their energy is not converted to useful output and only generates heat if absorbed. For photons with energy above the band gap energy, only a fraction of the energy above the band gap can be converted to useful output. When a photon of greater energy is absorbed, the excess energy above the band gap is converted to kinetic energy of the carrier. The excess kinetic energy is converted to heat through phonon interactions as the kinetic energy of the carriers

slows to equilibrium cell velocity (en.wikipedia.org/wiki/Solar cell; van der Lagemaat *et al.*, 2000).

Solar cells with multiple band gap absorber materials are able to more efficiently convert the solar spectrum. By using multiple band gaps, the solar spectrum may be broken down into smaller bins where the thermodynamic efficiency limit is higher for each bin (Wu *et al.*, 1983).

2.2.2 Maximum-Power Point

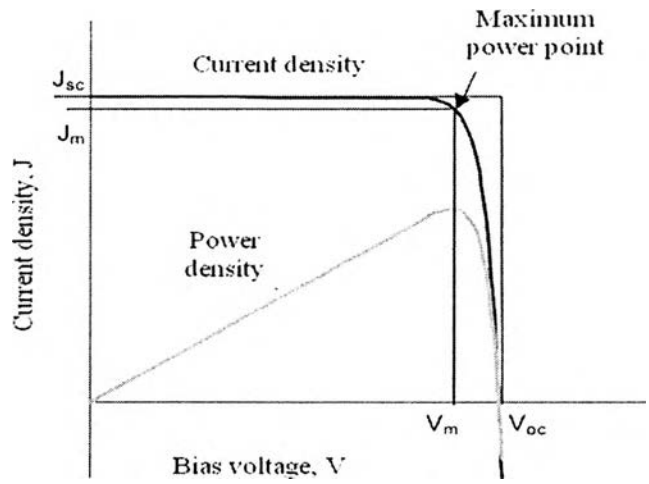

Figure 2.3 The current-voltage (black) and power-voltage (gray) characteristics of an ideal cell. Power density reaches a maximum at a bias V_m, close to V_{oc}. The maximum power density $J_m \times V_m$ is given by the area of the inner rectangle. The outer rectangle has area $J_{sc} \times V_{oc}$ (Nelson, 2004).

A solar cell can be operated over a wide range of voltages (V) and photo densities (J). The cell power density (P) is given by:

$$P = JV \tag{2.1}$$

P reaches a maximum at the cell's operating point or maximum power point P_m by increasing the resistive load on an irradiated cell continuously from zero

(a short circuit current, J_{sc}) to a very high value (an open circuit voltage, V_{oc}) one. This occurs at some voltage V_m with a corresponding current density J_m, as shown in Figure 2.3.

2.2.3 Fill Factor

The fill factor is a phenomenological quantity, which depends on the series resistance of the cell, which is the sum of the sheet resistance of the conducting glass substrate and counter electrode, the resistance of the substrate-TiO_2 interface, the resistance associated with ion transport in the electrolyte, the charge transfer resistance at the counter electrode, and the voltage dependence of the recombination rate (van der Lagemaat *et al*, 2000).

The fill factor of a solar cell/panel is the ratio of the solar cells actual power output (P_m) versus its 'dummy' power output (V_{oc} x J_{sc}).

$$FF = \frac{J_m V_m}{J_{sc} V_{oc}} \tag{2.2}$$

2.2.4 Energy Conversion Efficiency

The efficiency (η) of the cell is the power density delivered at operating point as a fraction of the incident light power density, P_s (Nelson, 2004):

$$\eta = \frac{J_m V_m}{P_s} \tag{2.3}$$

Efficiency is related to J_{sc} and V_{oc} using FF,

$$\eta = \frac{J_{sc} V_{oc} FF}{P_s} \tag{2.4}$$

These four quantities: J_{sc}, V_{oc}, FF, and η, are the key performance characteristics of solar cells. All of these should be defined for particular illumination

conditions. The Standard Test Condition (STC) for soar cells is the Air Mass 1.5 spectrum, an incident power density of 1000 Wm^{-2}, and a temperature of 25°C.

2.2.5 Parasitic Resistances

In real cells, power is dissipated through the resistance of the contacts and through leakage currents around the sides of the device. These effects are equivalent electrically to two parasitic in series (R_s) and in parallel or shunt (R_{sh}) with the cell.

The series resistance arises from the resistance of the cell material to current flow, particularly through the front surface to the contacts, and from resistive contacts. Series resistance is a particular problem at high current densities, for instance under concentrated light. The parallel or shunt resistance arises from leakage of current through the cell, around the edges of the device and between contacts of different polarity. It is a problem in poorly rectifying devices.

Series and parallel resistances reduce the fill factor, as shown in Figure 2.4. For an efficient cell, R_s needs to be as small, and R_{sh} needs to be as large as possible (Nelson, 2004).

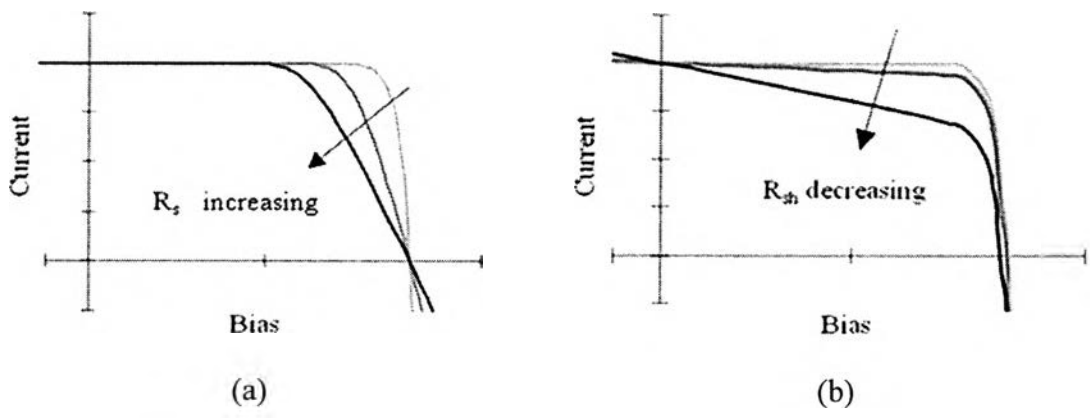

Figure 2.4 Effect of (a) increasing series and (b) reducing parallel resistances. In each case, the outer curve has $R_s = 0$ and R_{sh} = infinite. In each case, the effect of the resistances is to reduce the area of the maximum power rectangle compared to $J_{sc} \times V_{oc}$ (Nelson, 2004).

2.2.6 Dark Current

In general, dark current, back electron transfer reaction or recombination in solar cell happens when an injected electron recombines with a hole. However, in some case this path rarely occurs due to the limitation in time scale, for instance dye-sensitized solar cell, time used for an ultrafast electron injection from the dye to the TiO_2 electrode is less than 20 femtoseconds (Wenger *et al.*, 2005) and for fast dye regeneration via reduction by I^- is 100 nanoseconds (Haque *et al.*, 1998) while it needs milliseconds for an injected electron recombining with a hole or an oxidized dye. Alternatively, other pathways for this phenomenon occur between electrons in the conduction band of semiconductor oxides and electron acceptor in the electrolyte or between electrons at back electrode and acceptor in the electrolyte as described in Equation 2.5.

$$I_3^- + 2e \rightleftharpoons 3I^- \tag{2.5}$$

2.2.7 IPCE

The photocurrent action spectrum or the incident photon to current conversion efficiency (IPCE) as a function of wavelength is directly proportional to the number of electron output divided by the number of incident photons (Kay, 1994):

$$\text{IPCE} = \frac{n \text{ of electrons}}{n \text{ of photon}} = \frac{I/e}{P/hv} = \frac{I}{P}\cdot\frac{hc}{e\lambda} = \frac{I}{P}\cdot\frac{1240}{\lambda(\text{nm})} \tag{2.6}$$

An example of IPCE spectra was shown in Figure. 2.5 The IPCE can be express as the product of light harvesting efficiecy (LHE), the quantum yield of charge injection (Φ_{inj}) and the efficiency of collecting the injected charge at the back contact (η_c) (Nazeeruddin *et al.*, 1993; van der Lagemaat *et al.*, 2000; Zakeeruddin and Grätzel, 2009):

$$\text{IPCE}(\lambda) = \text{LHE}(\lambda)\,\Phi_{inj}\,\eta_c \tag{2.7}$$

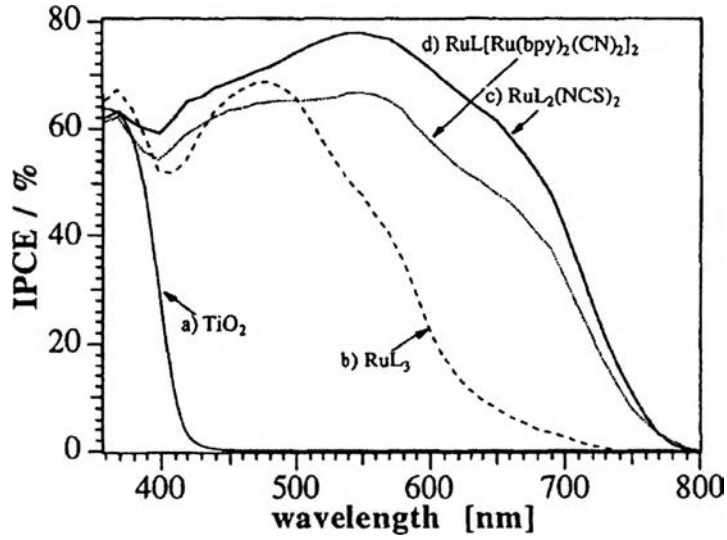

Figure 2.5 Photocurrent action spectra of TiO_2 electrodes (12 μm P25) sensitized with different Ru(II) bipyridine complexes, electrolyte: 80% ethlene carbonate, 20% propylene carbonate, 0.5 M KI, 40 mM I_2, a) bare TiO_2 electrode, b) RuL_3 (L= 2,2'-bipyridine-4,4'-dicarboxylate) adsorbed from water, pH 4.8, c) $RuL_2(NSC)_2$ and d) $RuL_2[Ru(bpy)_2(CN)_2]_2$ adsorbed from ethanol (Kay, 1994).

For dye-sensitized solar cell, all of these factors are related as described in the following description. "A low light harvesting efficiecy or light absorption can be due to, for example, a low dye concentration, a TiO_2 film too thin to absorp a significant fraction of the incident light, insufficient light scattering within the film, absorption of light by TiO_2 or the redox electrolyte, and dye degradation. A low quantum yield of charge injection can be due to, for instance, dye desorption, dye aggregation, higly perfect crystal plane of TiO_2 (Kay, 1994) or band edge movement. A low efficiency of collecting the injected charge at the back contact can be attributed to competiton between fast recombination of photoinjectied electrons with the redox electrolyte or oxidized dye and electron collection." (van der Lagemaat *et al.*, 2000)

2.3 Principle of Dye-Sensitized Solar Cells

Dye-sensitized solar cells separate the two functions provided by silicon in a traditional cell design. Normally, the silicon both acts as the source of photoelectrons, as well as provides the electric field to separate the charges and create a current. In the dye-sensitized solar cell, the bulk of the semiconductor is used solely for charge transport while the photoelectrons are provided from a separate photosensitive dye. Charge separation occurs at the surfaces between the dye, semiconductor, and electrolyte (www.dur.ac.uk/~dph0www5/solar.html.).

Sunlight enters the cell through the transparent conductive oxide top contact, striking the dye on the surface of the TiO_2. Electrons in the dye, which absorb enough energy, will jump to excited state of the dye, from which an electron can be "injected" directly into the conduction band of the TiO_2, and from there it moves by diffusion (as a result of an electron concentration gradient) to back electrode, as shown in Figure 2.6.

Meanwhile, the dye molecule has lost an electron, and the molecule will decompose if another electron is not provided. The dye strips one electron from iodide in electrolyte below the TiO_2, oxidizing it into triiodide. This reaction occurs quite quickly compared to the time that it takes for the injected electron to recombine with the oxidized dye molecule, preventing this recombination reaction that would effectively short-circuit the solar cell.

The triiodide then recovers its missing electron by mechanically diffusing to the bottom of the cell, where the counter electrode re-introduces the electrons, which flow back through the external circuit (www.dur.ac.uk/~ dph0www5/solar.html; Grätzel, 2001).

The photovoltage or V_{oc} of a cell is the different potential between quasi-Fermi level of electron in semiconductor in the light and Fermi level (E_f) of semiconductor in the dark which is equal to the redox potential in electrolyte or redox electrolyte energy (E_{redox}). At dark equilibrium, the E_f of TCO and the nanocrystalline semiconductor equals E_{redox} (Frank, 2004; Schlichthörl *et al.*, 1997). Under illumination, a number of injected electrons from the excited state of the dye in the conduction band of the nanocrystalline semiconductor rise up the quasi-Fermi

level of electron. Therefore, "The quasi-Fermi level in the light is controlled by the light-harvesting efficiency of the dye, the quantum yield of electron injection and the time constant for recombination with the electron acceptor, i.e. triiodide, oxidized dye." (Frank 2004) At open circuit, E_f of TCO equals E_f of the nanocrystalline semiconductor. (Schlichthörl *et al.*, 1997)

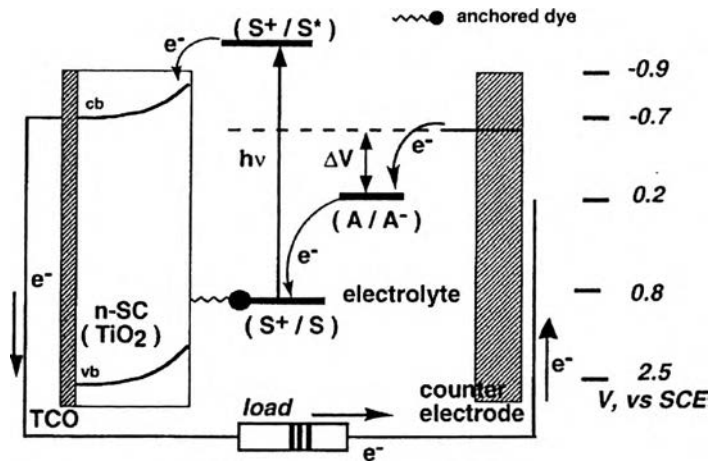

Figure 2.6 Principle of operation of dye-sensitized solar cell (Kalyanasundaram and Grätzel, 1998).

2.4 Band-Edge Movement

Apart from the changing of electron concentration due to electron photoinjection and electron recombination in conduction band changing V_{oc}, an important phenomenon affecting V_{oc} is band-edge movement with respect to E_{redox} (Kopidakis *et al.*, 2006). Band-edge movement occurs with a change in the potential drop across the Helmholtz layer.

"An example of band-edge movement, which probably caused by photoinjection of electrons in conduction band leading to a change of the electric field across the Helmholtz layer is depicted in Figure 2.7. The redox energy of the ground state $E(D^+/D)$ and excited state $E(D^+/D^*)$ of the dye, the conduction-band edge of the nanocrystalline semiconductor (E_{cb}) and transparent conducting oxide

substrate (E_{cb}(TCO)) are referenced to E_{redox}. For a highly doped TCO, Fermi energy (E_f) lies close to E_{cb}(TCO). Under illumination, the injected electrons from excited state of dye molecules accumulate in the conduction band (CB) and surface state (SS) of semiconductor." (Schlichthörl *et al.*, 1997)

"Q_{cb} determines the difference between E_f and E_{cb} of the semiconductor. Because Q_{cb} fixes the position of E_f with respect to E_{cb}, a shift of E_{cb} will be accompanied by an equal displacement of E_f relative to E_{redox}." (Schlichthörl *et al.*, 1997) As a result, V_{oc} changes with band-edge movement (ΔE_{cb}).

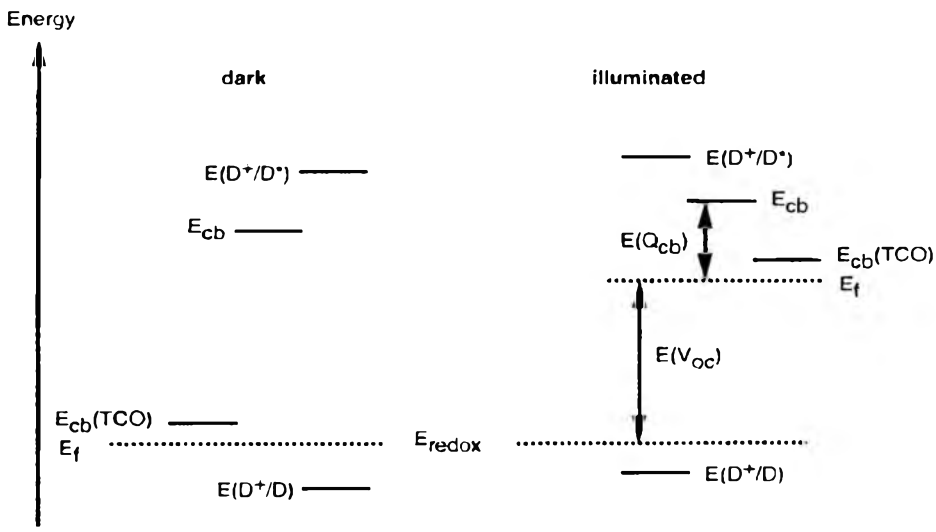

Figure 2.7 Energy-level diagram of a dye-sensitized nanocrystalline semiconductor solar cell (Schlichthörl *et al.*, 1997).

The change in the potential drop across the Helmholtz layer possibly arises from the accumulation of photoinjected electrons at surface states, the accumulation of photoinjected electrons in conduction band changing the electric field by inducing accumulation of compensating positively charged ions at semiconductor/electrolyte interface, or charge building up on the surface of semiconductor owing to chemical treatment. (Kopidakis *et al.*, 2006; Schlichthörl *et al.*, 1997)

A sufficient net number of charges build up on the surface of the particles in order to induce a change in the potential drop across Helmholtz layer. A negative surface charge (negative charging or deprotonating) can cause the band edges to shift

upward, toward negative electrochemical potentials, leading to a higher photovoltage. Conversely, a positive surface charge (or dipole) buildup (positive charging or protonating) can cause the conduction band edge to move downward, toward positive potentials, favoring a lower photovoltage." (Kopidakis *et al.*, 2006)

"The accumulation of photoinjected electrons at surface states can cause the potential drop across Helmholtz layer when surface state capacity (C_{ss}) is in the same magnitude with Helmholtz layer capacity (C_H). However, in practical photoelectrochemical cells, C_{ss} is much smaller than C_H. Meanwhile, an upper limit for the potential drop across the accumulation layer is determined by the strength of the electric field at the semiconductor surface induced by cations from solution, which compensate the charge of photoinjected electrons. But less of electric field is generated due to the restriction of their small particle size in nanoscale, the surface-charge density, the photoinduced free-carrier concentration in the conduction band, and the doping density of the particle. Accordingly, the contribution of electric field to the photovoltage is negligible." (Schlichthörl *et al.*, 1997) As a consequence, the chemical treatment influences most to the band-edge movement at a fixed photoinduced charge density.

2.5 Components of Dye-Sensitized Solar Cells

2.5.1 Photosensitizers

"The ideal sensitizer for a single junction photovoltaic cell converting standard global air mass 1.5 sunlight to electricity should absorb all lights below a threshold wavelength of about 920 nm. In addition, it must carry attachment groups or anchoring groups, such as carboxylate or phosphonate to firmly graft it to the semiconductor oxide surface. However, the electrons move through the carboxylic acid anchor two times faster than through the phosphonic anchor (Lee *et al.*, 2011). Upon excitation, it should inject electrons into the solid with a quantum yield of unity. The energy level of the excited state should be well matched to the lower bound of the conduction band of the oxide to minimize energetic losses during the electron transfer reaction. Its redox potential should be sufficiently high that it can be regenerated via electron donation from the redox electrolyte or the hole conductor.

Finally, it should be stable enough to sustain about 10^8 turnover cycles corresponding to about 20 years of exposure to natural light." (Grätzel, 2003)

A sensitizer, dye, or pigment consists of a part called chromophore which functions as a certain wavelength of visible light absorber and others reflector. Chromophore can be classified into 2 types which are conjugated π systems and metal complex.

Conjugated chromophore is a series of alternating single and double bonds which have overlapping of p-orbitals with delocalized π electrons across all the adjacent aligned p-orbitals. Besides the alternating single and double bonds, the conjugated systems can contain electron lone pairs, carbanium ions (CR_3+), carbonyl groups (C=O), imine groups (C=N), and etc. In general, these conjugated structure lower the energy different between two different molecular orbitals (HOMO to LUMO or herein π to π*) according to the length of conjugated system as shown in Fig. 2.8. Consequently, extending a conjugated system will tend to shift absorption to longer wavelengths. (en.wikipedia.org/wiki/Chromophore,)

Metal complex chromophore stems from the splitting of d-orbitals by binding of a transition metal to ligands. The examples can be four pyrroles arranged as a porphyrin ring with a central metal atom, such as chlorophylls, hemoglobin, and etc. In general, they have two kinds of intramolecular charge transfer: ligan to metal charge transfer (LMCT) and metal to ligan charge transfer (MLCT). For n-type DSSC, the MLCT mechanism is involved. The MLCT transition corresponds to promotion of an electron from a molecular orbital (MO) that is largely metal based (such as electron filled t_{2g} level of Ru(II)) to a MO that is largely ligan based (empty π* orbital of the ligan).

Apart from chromophore, dye usually has auxochromes attached to a chromophore. Auxochrome is a functional group of atoms with electron lone pairs, such as carboxylic acid (-COOH), hydroxyl (-OH), sulfonic acid ($-SO_3H$), primary amine ($-NH_2$), secondary amine (-NHR), tertiary amine ($-NR_2$), and etc. If these groups are in direct conjugation with π-system of the chromophore, they can increase the wavelength of absorption since their electron lone pairs are considered to extend the conjugated system, and also intensify the absorption. Moreover, an auxochrome

assists a dye to bind to the object that is colored or it can be called an anchoring group.

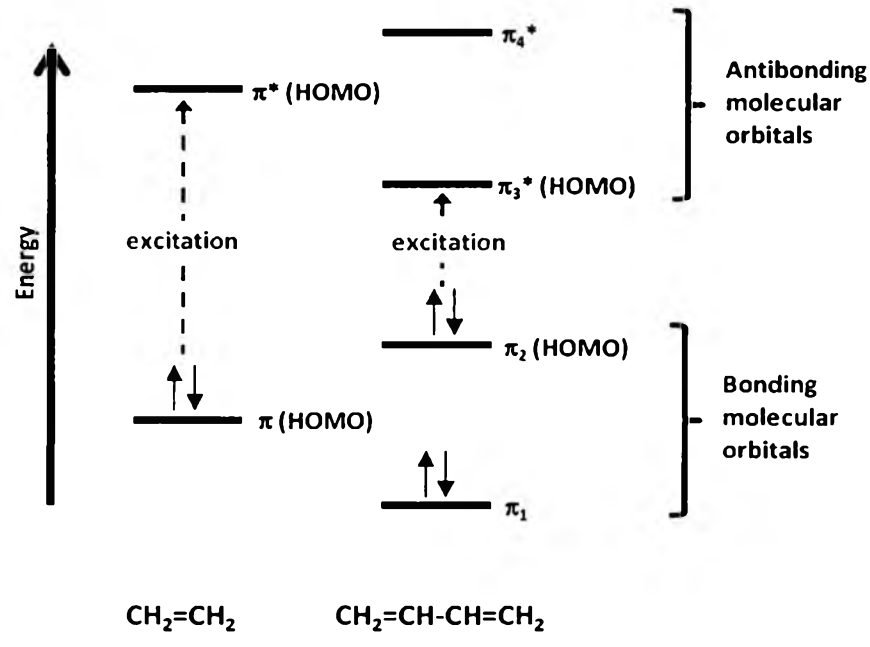

Figure 2.8 The relative energies of the π molecular orbitals of ethane and 1,3-butadiene. (Graham Solomons, 1990)

The auxochrome can be classified to electron donor and electron acceptor or electron-withdrawing group. In molecular engineering, the energy level of both HOMO and LUMO can be altered by substitution of these auxochromes on a chromophore. For instance, electron donor raises HOMO level; instead, electron acceptor lowers LUMO level. However, both phenomena then lower the energy gap. The examples of electron donor are amine derivative ($-NR_3$), ether (-OR), hydroxyl (-OH), thiocyanate (-NCS), and etc. Meanwhile, electron acceptors are carboxylic (-COOH), ester (-COOR), sulfonic acid ($-SO_3H$), phosphonic acid ($-PO_3H$), cyanide (-CN) and etc. Some of them can be anchoring groups as well, such as hydroxyl and acid groups. In n-type DSSC, the position of electron acceptor locates normally at the anchoring side such that it can determine the charge transfer direction, which is general from donor to accepter, and provide the high electron density at the surface

of semiconductor to facilitate photoinjection of excited electron from dye molecules (Qin, 2010).

Dyes or photosensitizers used in research today can be divided into two main types: synthetic dyes and natural dyes. For synthetic dyes, highly efficient dyes are based on Ru(II) complexs (Kalyanasundaram and Grätzel, 1998; Grätzel, 2003), which contain heavy metal. Besides, organic dyes with various structures and anchoring groups (Chen *et al.*, 2005; Zakeeruddin and Grätzel, 2009) are very interesting.

2.5.1.1 Ruthenium(II) Based Dyes

The dyes currently used are sensitive in wide frequency from UV to IR light, especially "triscarboxy-ruthenium terpyridine" [Ru(4,4',4"-$(COOH)_3$-terpy)$(NCS)_3$]. The wide spectral response results in the dye having a deep brown-black color, and is referred to simply as "black dye" (Figure 2.9) (Nazeeruddin *et al.*, 2001). The black dye was developed from high efficient homoleptic sensitizers, N719 and N3 (Nazeeruddin *et al.*, 1993), which contain different degree of protonation (Figure 2.9), in order to enhance the red and near infrared region adsorption but itself loses the molar extinction coefficient (ε_{max}). Hence, it needs thicker film to achieve high DSSC performance. In addition, the degree of protonation of sensitizers is an important factor to optimize the DSSC performance since it influences directly to the TiO_2 band edge movement. The protonated sensitizer charges the TiO_2 surface positively by transferring its protons upon adsorption. This enhances the adsorption of the anionic ruthenium complex and assists electron injection from the excited state of the sensitizer into the TiO_2 conduction band, favoring high photocurrents. However, the V_{oc} is lowered due to the positive shift of the conduction band edge induced by the surface protonation. In contrast, if the degree of protonation decreases, the high V_{oc} will take place due to the relative negative shift of the conduction band edge induced by the adsorption of the anionic complex, but as a consequence the J_{sc} is lower. Thus, there should be an optimal degree of protonation of the sensitizer to maximize the product of J_{sc} and V_{oc}.

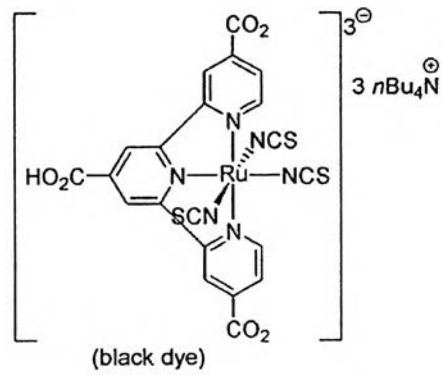

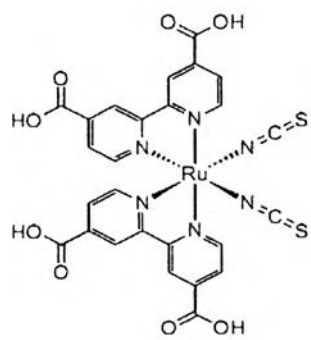

N3

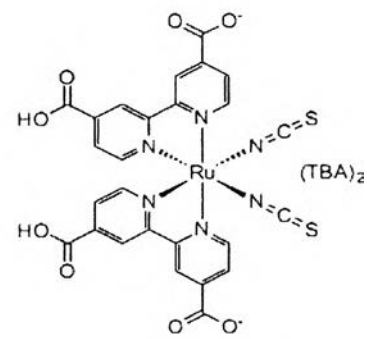

N719

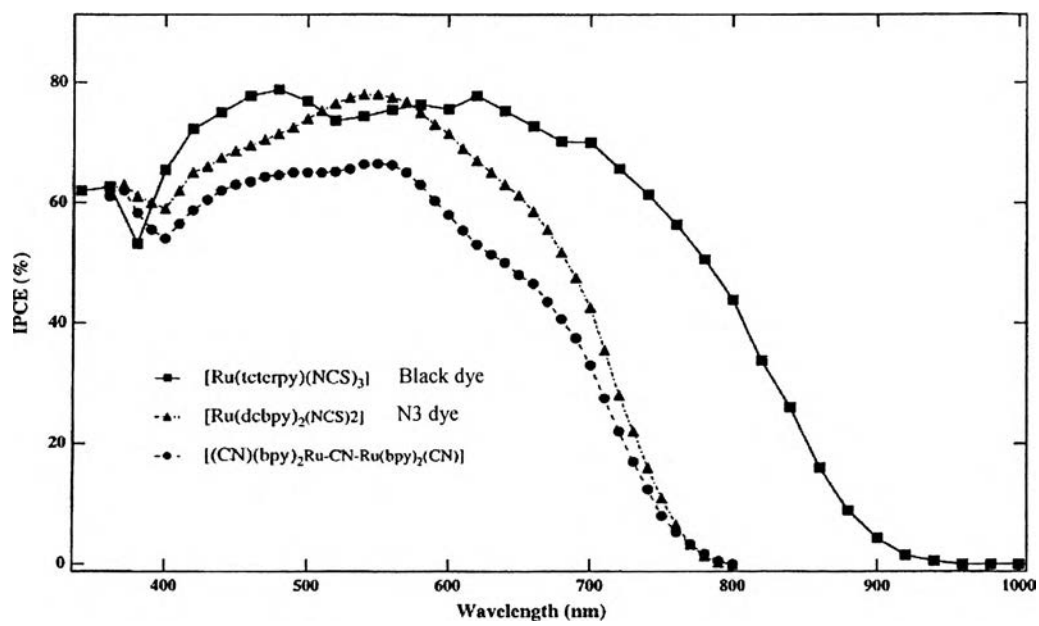

Figure 2.9 Molecular structure of ruthinium (II) dyes N3, N719 and Black dye, and IPCE spectra of N3 and black dye (Kalyanasundaram and Grätzel, 1998; Vougioukalakis *et al.*, 2010).

Table 2.1 Spectral data and photovoltaic efficiency of rutinium-based dyes with acetonitrile-based electrolyte

Dye	Absorption maximum wavelength [nm]	Maximum molar extinction coefficient [$M^{-1}cm^{-1}$]	Efficiency
N719	534	14000	11.18% [I,a],5.0% [II,b]
Black dye	600	7640	11.1% [I,c]
Z907	524	12200	6.6% [II,b]
K19	543	18200 t-butanol+ AN1:1	N/A
K77	546	19400 DMF	10.5% [I,d], 9% [II,d]
C101	547	17500 DMF	11.0% [I,e], 7.41% [II,e]
C102	547	16800 DMF	9.5% [I,e]
C103	550	18800 DMF	8.5% [II,f]
CYC-B1	553	212000	8.54% [g]
CYC-B11	554	24200	11.5% [I,h]
CYC-B13	547	19300	9.6% [I,i]

[I]Volatile-based electrolyte, [II]Ionic liquid electrolyte.

[a] Nazeeruddin *et al.*, 2005, [b] Wang *et al.*, 2003a, [c] Chiba *et al.*, 2006, [d] Kuang *et al.*, 2007, [e] Gao *et al.*, 2008, [f] Shi *et al.*, 2008, [g] Chen *et al.*, 2006, [h] Chen *et al.*, 2009a, [i]Chen *et al.*, 2009b

Since the high number of carboxylic groups in homoleptic sensitizers is easily attacked by water and then causes dye desorption during light soaking (Wang *et al.*, 2003b; Vougioukalakis *et al.*, 2010), this deteriorates the long term stability of DSSCs which is difficult to make the DSSC practical. The heteroleptic sensitizers with two hydrophobic chains replacing two carboxylic groups such represented by Z907 (Figure 2.10) were approved to prolong cell life time under thermal stress (Zakeeruddin *et al.*, 2002; Wang *et al.*, 2003c). Besides, the incorporated hydrophobic chain can prevent water attraction and contribute the cell stability, and it can retard the recombination process and prolong the electron life

time by shielding the TiO_2 surface from the redox mediator (Wang *et al.*, 2003a; Cao *et al.*, 2009). This leads to increasing V_{oc} and the cell performances, in particular the cell with solvent-free or ionic liquid electrolytes which comprise of high I_3^- concentration and low dye regeneration rate due to high viscosity of the system. Comparing high efficient dye N719 with Z907, Wang *et al.* (2003a) found that cells with the standard N719 dye showed lower total conversion efficiencies due to faster back transfer of electrons from the conduction band of the TiO_2 film to I_3^-, which lowers the V_{oc}. Nevertheless, Z907 dye provided low molar extinction coefficient which results in low J_{sc}. Thus, there were many attempts to increase the molar extinction of these heteroleptic dyes or amphiphilic dyes in order to enhance the cell performances along with the cell stability. Several heteroleptic dyes are shown in the Figure 2.10. The strategy to accomplish the high molar extinction coefficient of sensitizers is to extend π conjugation of the hydrophobic parts, for instance K19 (Wang *et al.*, 2005) and K77 (Kuang *et al.*, 2007) or C101 (Gao *et al.*, 2008) with π conjugation of electron rich thiophene derivative and CYC-B11 (Chen *et al.*, 2009a), etc. These high stable dyes with high molar extinction coefficient improved the DSSC efficiency up to 11%. The molar extinction coefficient and cell efficiency of ruthenium-based dye are shown in Table 2.1. Likewise, these sensitizers with high molar extinction coefficient are adequate for thinner TiO_2 film (2-5 μm). This is a great benefit for solid-state DSSCs with hole transport materials (HTM) like 2,2,7,7-tetrakis-(*N,N*-di-*p*-meth nanoparoxyphenyl amine)-9,9-*spiro*bifluorene or spiro-OMeTAD which would be mentioned in section 2.5.3.2 (Chen *et al.*, 2009a; Chen *et al.*, 2009b; Cai *et al.*, 2011). However, the drawbacks of ruthenium based dye are not only based on the environmentally friendly problem and its expensive cost, but also the limitation in increasing the molar extinction coefficient (Zakeeruddin and Grätzel, 2009) and tuning the absorbing light spectrum (Lee *et al.*, 2011).

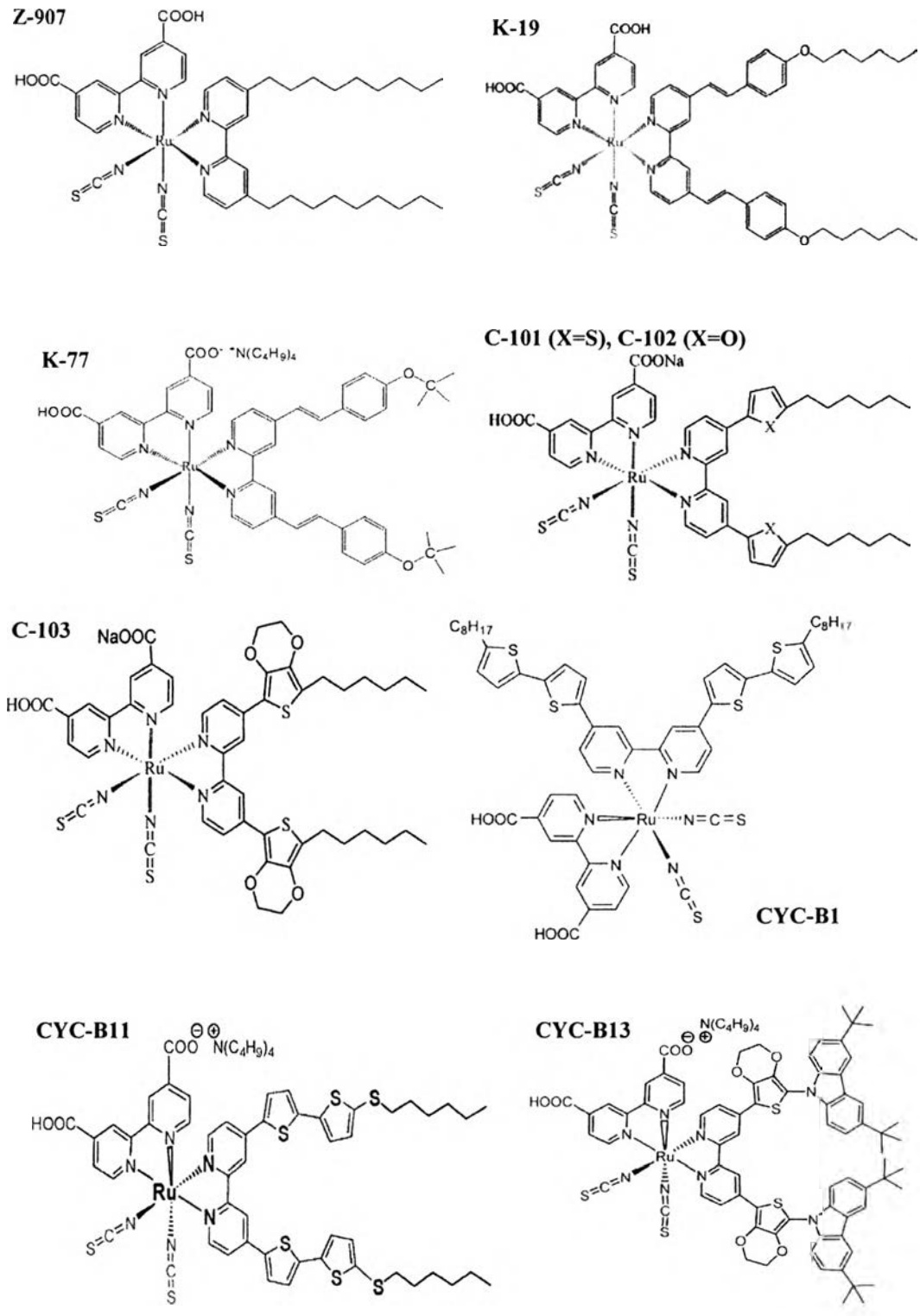

Figure 2.10 Molecular structure of heteroleptic ruthinium-based dyes.

2.5.1.2 Organic Dyes

The organic dyes or metal-free organic sensitizers could resolve ruthenium-based dye problems above. Their molar extinction coefficients are typically two to three times higher than those of ruthenium complex (Zakeeruddin and Grätzel, 2009). They consist of electron donor, electron acceptor, conjugated spacer between electron donor and electron acceptor, and surface anchoring group (Lee *et al.*, 2011). In that manner they are usually called "D–π–A organic dyes". The photovoltaic performances of cells with this kind of dye afford very close to those of cells with ruthenium complex.

Two main interesting parameters, the red shift and high molar extinction coefficient have been adjusted by tailoring the dye structure to improve organic dye performances. To accomplish the red shift adsorption, the stronger electron donating alkoxy group is introduced to the donor part such the increase in red spectral response from C207 to C202 and C208 (Xu *et al.*, 2008). Various organic dye structures are shown in Figure 2.11 and the optical characteristics along with cell efficiency of these organic dyes are listed in Table 2.2. The most effective way to enhance both red shift spectra and high molar extinction is still to extend π system of spacer, which also reduces the solubility of organic dye in the electrolyte. For example, the modification of D102, C201, C206, and JK45 to D149, C203, C211, and JK 46 facilitated the high incident photon to current conversion efficiency at red spectral range and then high cell efficiency. Besides, the addition of alkyl group on the structure contributes the longer electron life time in the TiO_2 film and therefore high V_{oc}, for instance, the addition of alkyl chain on D149, C202 and JK2 to obtain D205, JK45 and C206, respectively. These alkyl groups also improved the cell stability. From this point of view, it is interesting to see that most of efficient organic dyes contain sulfur compound which is against the environmental. Therefore, in this circumstance the existence of environmentally issue still challenges the researchers to overcome.

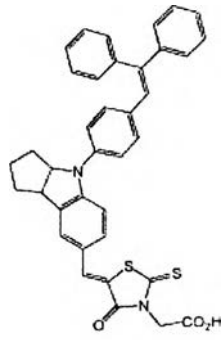

D102

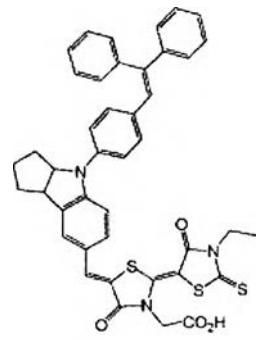

D149

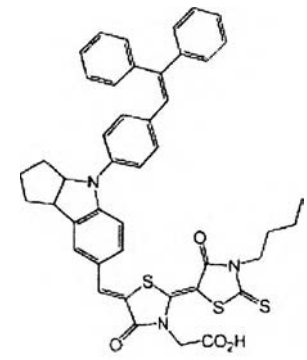

D205

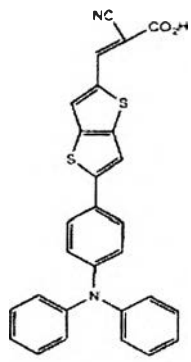

C207

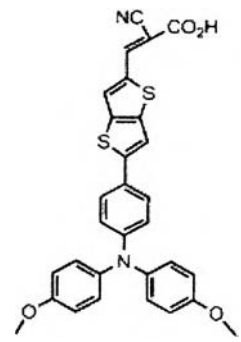

C202

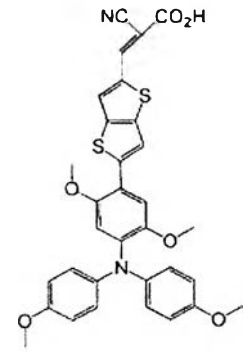

C208

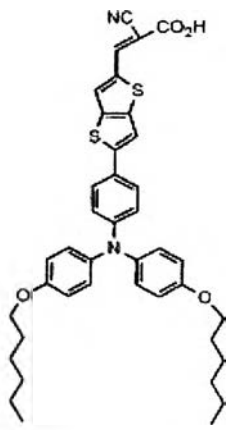

C206

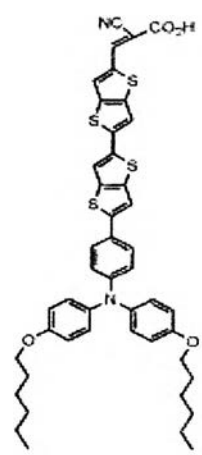

C211

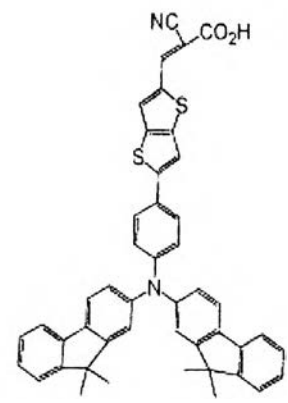

C201

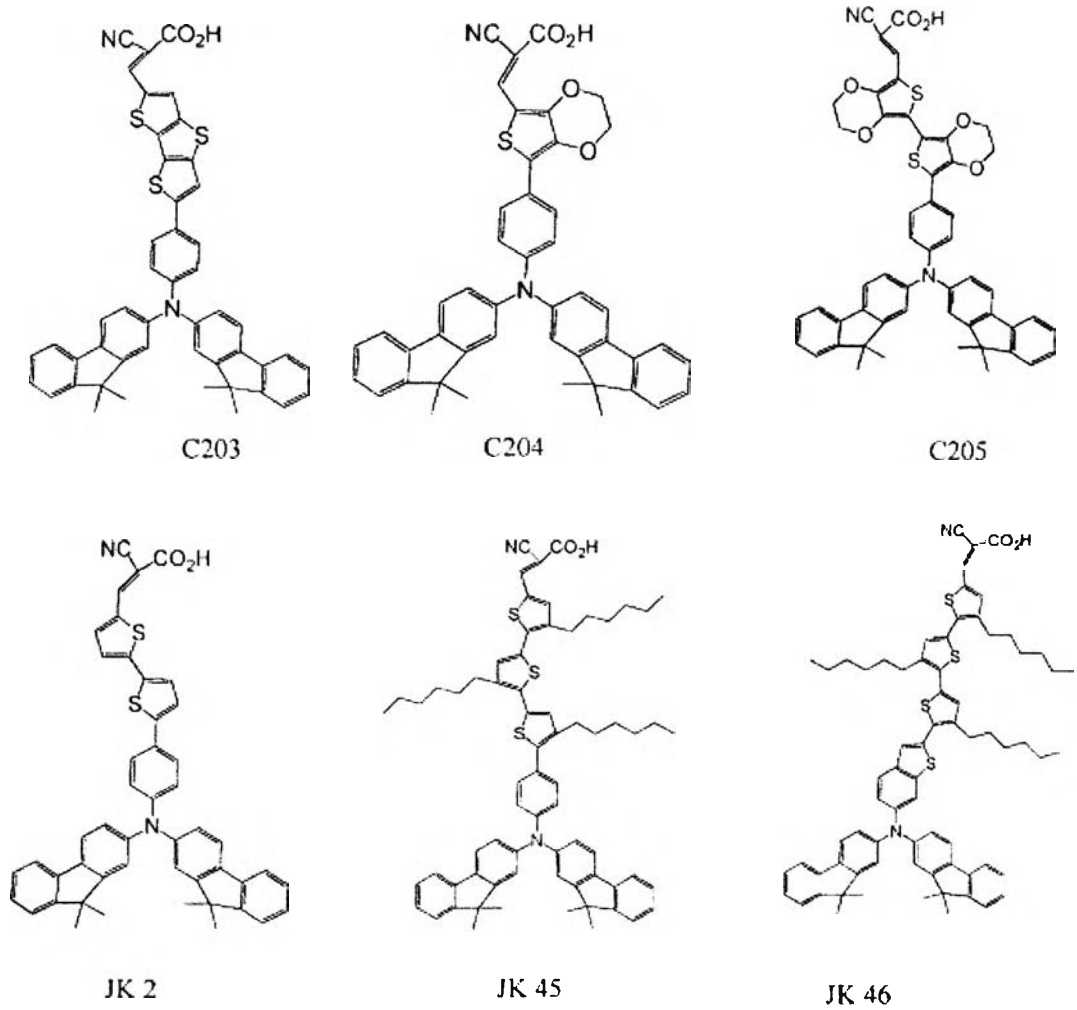

Figure 2.11 The molecular structure of organic dyes (Zakeeruddin and Grätzel, 2009).

Table 2.2 Spectral data and photovoltaic efficiency of organic dyes with ionic liquid electrolyte (Zakeeruddin and Grätzel, 2009)

Dye	Absorption maximum wavelength [nm]	Maximum molar extinction coefficient [$M^{-1}cm^{-1}$]	Efficiency
C201	514	41200 $CHCl_3$	7.00
C202	512	40500 $CHCl_3$	6.54
C203	525	44800 $CHCl_3$	7.00
C204	525	33500 $CHCl_3$	7.31
C205	544	38500 $CHCl_3$	7.61
C206	516	41900 $CHCl_3$	7.05
C207	493	36600 $CHCl_3$	5.93
C208	517	33700 $CHCl_3$	6.80
C211	524	47000 $CHCl_3$	6.50
D102	494	61000 THF	4.85
D149	526	68700 t-butanol+ AN1:1	6.38
D205	532	53000 THF	7.18
JK2	452	39000 EtOH	6.02

2.5.1.3 Natural Dyes

On the contrary, the main structure of natural dyes come from anthocyanin group (Figure 2.12) (Calogero *et al.*, 2008; Furukawa *et al.*, 2009; Garcia *et al.*, 2003; Hao *et al.*, 2006; Kumara *et al.*, 2006; Polo *et al.*,2006; Wongcharee *et al.*, 2007), which is found most in fruits and has various colors. The other groups are betalain (Figure 2.13) (Zhang *et al.*, 2008; Calogero *et al.*; 2010), carotenoid (Figure 2.14) (Yamazaki *et al.*, 2007) and chlorophyll (Fig. 2.15) (Chang *et al.*, 2010; Hao *et al.*, 2006; Kay and Grätzel, 1993; Kumara *et al.*, 2006). Now the best cell performances are obtained from raw betalain dyes extracted from red turnip (Calogero *et al.*, 2010), of which the J_{sc} is 9.5 mA/cm^2, V_{oc} is 425 mV, *FF* is 0.37, and η is 1.7% with 0.5 M LiI/0.05M I_2 electrolyte and (5-6μm) transparent TiO_2 film.

Since environment concern is an importance issue, many researchers have tried to develop DSSC sensitized with natural dyes, which still provide low efficiency due to low light absorption in the whole visible region range, weak binding energy with TiO_2 film (Chang *et al.*, 2010), and high electron recombination, and low stability. The weak binding energy stems from the lack of anchoring groups, such dyes in chlorophyll and carotenoid groups. Besides, strong steric hindrance of the bulky structure or very long alkyl chain could prevent dye arraying on TiO_2 surface efficiently (Hao *et al.*, 2006; Wongcharee *et al.*, 2007). The interaction between natural dyes and TiO_2 surface is exhibited by the broadening and the red shift of the absorption band of dye adsorbed on TiO_2 surface. As a result, the absorption band shifts to lower energy, owing to the electronic coupling between the adsorbed dyes and TiO_2 (Calogero and Marco, 2008; Kay 1994, Polo and Iha, 2006; Vougioukalakisa *et al.*, 2011; Wongcharee *et al.*, 2007).

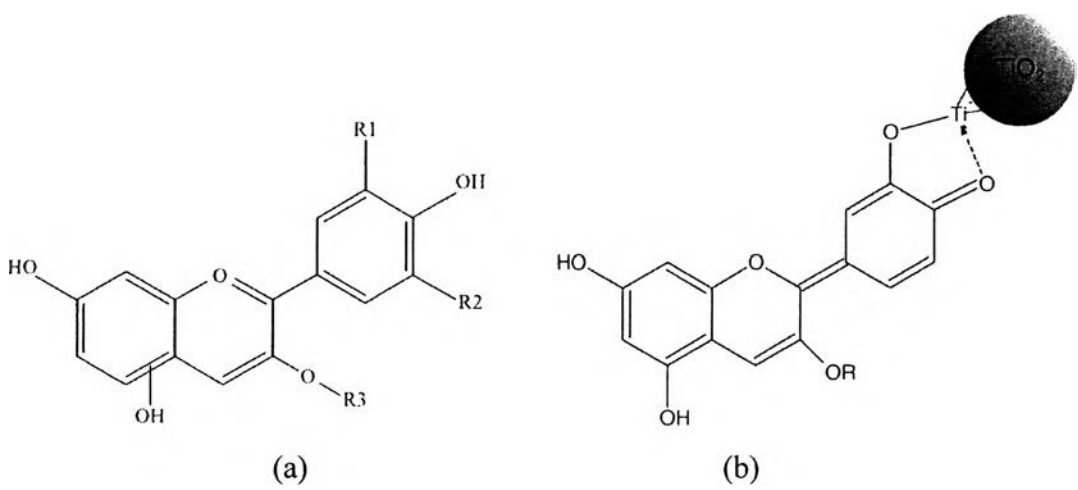

Figure 2.12 Schematics of (a) anthocyanin structure (Wongcharee *et al.*, 2007), and (b) the binding between anthocyanin and TiO_2 particles (Hao *et al.*, 2006).

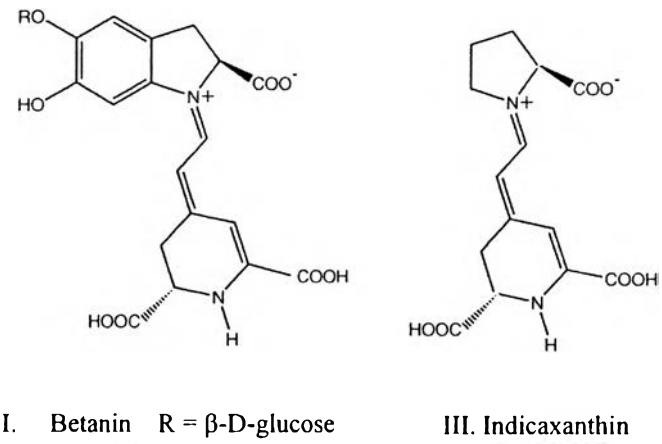

I. Betanin R = β-D-glucose
II. Betanidin R = H

III. Indicaxanthin

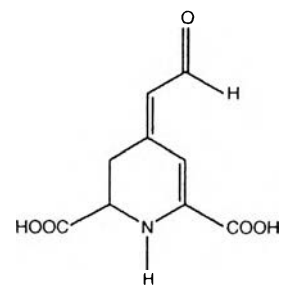

IV. Betalamic Acid

Figure 2.13 Betalain pigments (Zhang *et al.*, 2008).

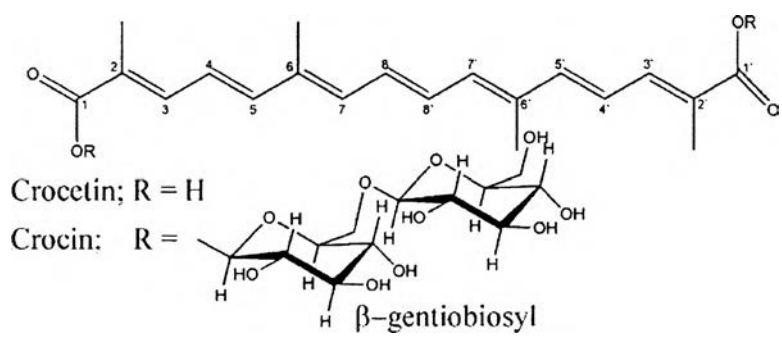

Figure 2.14 Carotenoid structures (Yamazaki *et al.*, 2007).

Nevertheless, the high recombination and low electron injection efficiency due to quenching of the excited state of natural dyes are attributed to a dye aggregation (Lee and Yang, 2011). Lee and Yang (2011) mentioned that this phenomenon could be observed in ruthenium based-dyes with a

large number of carboxyl groups, which have chances to form intermolecular aggregation from hydrogen bonding between carboxyl groups. Also, the dye aggregation is the main drawback of organic dyes as Liu *et al.*, (1997) reported. In case of natural dye, this could be seen from broadening shape of visible absorption spectrum of natural dye adsorbed on TiO_2 (Kay 1994; Vougioukalakisa *et al.*, 2011). To solve this, use of coadsorbates, such as organic acids with carboxyl group (Calogero *et al.*, 2010; Kay 1994) was the way. However, acid results in lowering the V_{oc} due to positive shift of TiO_2 Fermi level (Calogero *et al.*, 2010).

Since the natural dyes are sensitive to pH, solvent, temperature, and oxygen (antioxidant), these factors influence much to the cell performances and the cell stability. Chang *et al.* (2010) and Wongcharee *et al.* (2007) found that the efficiency of cell with anthocyanin dyes improved with decreasing pH and reached a maximum at the optimum pH 1.0. This was ascribed to higher J_{sc}, corresponding to higher light absorption. As a result, protonation of proton on TiO_2 surface would enhance dye adsorption. Nevertheless, this influenced to lowering V_{oc} as mention above. Besides, Chang *et al.* (2010) found the blue shift under acidic environment along with improvement of the fill factor. In addition, at pH 1.0 the cell stability was better because anthocyanin existed as flavylium ion, which is stable form of anthocyanin. However, at pH lower than 1.0 the cell efficiency was deteriorated by acid leaching.

Wongcharee *et al.* (2007) reported that ethanol as extract solvent provided better efficiency than water since anthocyanin is more soluble in ethanol, i.e. good dispersion and less aggregation of dye molecule. Nevertheless, the cell stability of the ethanol system deteriorated quicker after exposed to the simulated sun light for 3 h compared to that of water system. This was ascribed to faster photocatalytic decomposition of dye on TiO_2 in the presence of ethanol. Kay (1994) found that chlorophyll a as shown in Figure 2.15 did not adsorb efficiently on TiO_2 from solvent like ethanol, acetone, THF, or pyridine, due to the week interaction of its ester and keto carbonyl groups with the hydrophilic oxide surface but it did adsorb from less polar solvent like diethyl ether or hexane. Moreover, he found that Cu-2-α-oxymesoisochorin e_4 (Figure 2.16), the major product from hot saponification of raw chlorophyll in the presence of a copper salt, adsorbed on TiO_2 efficiently in more

polar methanol than in less polar solvent like acetone, propylene carbonate, dioxane, pyridine, or THF. However, coadsorption of Cu-2-α-oxymesoisochorin e_4 with coadsorbates like cholic acid (Figure 2.17) in ethanol solution was obtained better efficiency.

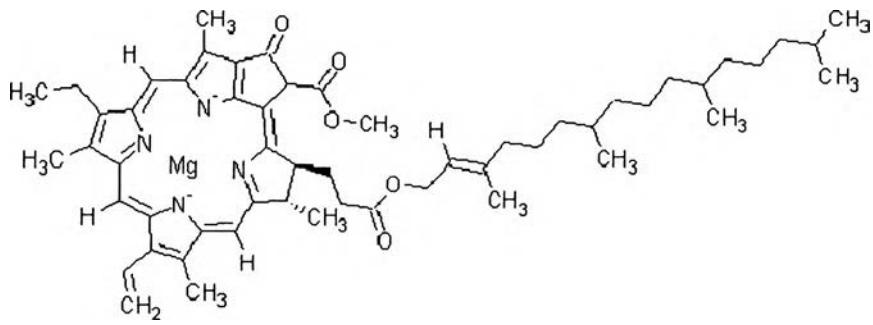

Figure 2.15 The chemical structure of chlorophyll a.

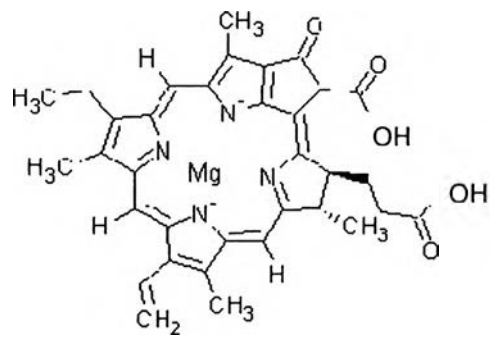

Figure 2.16 The chemical structure of Cu-2-α-oxymesoisochorin e_4.

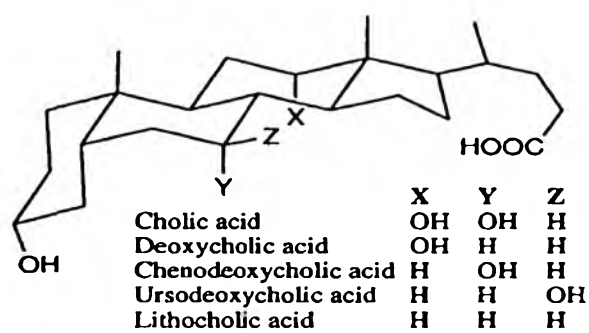

	X	Y	Z
Cholic acid	OH	OH	H
Deoxycholic acid	OH	H	H
Chenodeoxycholic acid	H	OH	H
Ursodeoxycholic acid	H	H	OH
Lithocholic acid	H	H	H

Figure 2.17 The chemical structures of cholic acid and its derivatives (Kay, 1994).

Meanwhile, extraction temperature would influence to dye concentration and dye stability as the studies of Chang *et al.* (2010) and Wongcharee *et al.* (2007) since the efficiencies increased with extraction temperature till 50 °C. The decrease in cell performance at higher extraction temperature was the result of faster degradation rate of dye. As most of natural dyes, especially dye in anthocyanin group are strong antioxidants, avoiding of dye exposed to the oxygen is needed during the cell preparation, i.e. under inert gas, or adding another stronger antioxidant is probably a choice. Nevertheless, some antioxidant like benzoquinone adsorbed next to the dye molecule may either quench the excited sensitizer or recombine with the injected electron, resulting in diminishing sensitization efficiency (Kay 1994).

2.5.2 Photoanode or n-Type Semiconductor

The n-type semiconductor surfaces act as the host matrix/support, for example, TiO_2, ZnO, Nb_2O_5, WO_3, Ta_2O_5, CdS, and CdSe. Those with band gap energy $\geq$ 3.0 eV are nearly transparent to major part of the solar spectrum. Band gap excitation leads to generation of holes in the valence band along with the electrons in the conduction band. Oxides have been widely used for their exceptional stability against photo-corrosion on optical excitation in the bandgap (Kalyanasundaram and Grätzel, 1998).

The performance of DSSC also depends on the key parameters of the n-type semiconductor, such as porosity, pore size distribution, light scattering, and electron percolation (Lee *et al.*, 2006b). In highly porous nano-textured films and small particle size, the available surface area for dye adsorption can be enormous. Porosity is another factor that needs to be optimized. For the fast regeneration of the oxidized dye and charge transport, the redox electrolyte must be able to penetrate the pores efficiently and be present in places, where the dye resides (Barbé *et al.*, 1997). The larger the particle size, the larger will be the porosity of the layer. The larger particles also scatter the incident radiation more effectively, and this has been found to be a positive factor in enhancing the red-light response of the sensitizer (Ferber and Luther, 1998; Hore *et al.*; 2006, Usami, 2000; Wang *et al.*, 2004a). So, the preparation procedure must be optimized in order to provide an optimal particle size

and porosity features. Sintering of the particles that form the film is another important step related to electron percolation within the film and reducing of dark currents (Nazeeruddin *et al.*, 1993). Sintering produces low resistance ohmic contacts between the particles, and between the particles and the conductive layer on glass substrate (Grätzel, 2003). Thus, the electrons injected anywhere within the network of particles can hop through several particles and reach the back contact without being lost (trapped) within the oxide layer. The injected electron has to be transported across a large number of colloidal particles and grain boundaries. There will be an increased probability of recombination with increased film thickness. Consequently, there exists an optimal thickness to obtain maximum photocurrent (Ferber *et al.*, 1998; Haung *et al.*, 2006; Ito *et al.*, 2008; Ito *et al.*, 2009; Wang *et al.*, 2004a). Usually, the optimum thickness for DSSC is in the range of 2-25 μm, also depending on molar extinction coefficient of dyes, and types of hole conductor materials. The too thick film leads to a decrease in photovoltage and fill factor (Kalyanasundaram and Grätzel, 1998; Nazeeruddin *et al.*, 1993).

Amongst oxide semiconductors, titanium dioxide (TiO_2), a white pigment, is by far the most commonly used. As a cheap and readily available material, TiO_2 serves as an attractive candidate for many industrial applications (paints, paper, coatings, plastics, fibers, cosmetics, etc.). Such films are of interest in anti-reflection coatings, dielectric materials, sensors, and waveguides. It is a wide band gap semiconductor with band gap energy being ca. 3.2 eV. Rutile, anatase, and brookite are the three common crystalline polymorphs of TiO_2. Rutile is the thermodynamically most stable polymorph (ca. 1.2–2.8 kcal mol^{-1} more stable than anatase). Anatase to rutile transformation occurs in the temperature range 700–1000°C, depending on the crystallite size and impurity content. The band gap energies for anatase and rutile have been estimated to be 3.2 and 3.0 eV, respectively (Kalyanasundaram and Grätzel, 1998). In DSSC, anatase phase is preferable due to higher electron transportation (Pavasupree *et al.*, 2006; Wang *et al.*, 2004a).

There are several methods of TiO_2 paste preparation employed for DSSC. Three of them have been commonly used in the literatures. The first one is preparing a TiO_2 paste from TiO_2 powder. The commercial TiO_2 powder or synthetic TiO_2 powder is ground with binder, surfactant, dispersant, stabilizer, solvent, etc to

make the paste (Nazeeruddin *et al.*, 1993; Xie *et al.*, 2007; Fan *et al.*, 2010; Ma *et al.*, 2003). The second one is preparing the paste from synthetic TiO_2 colloid blended with binder and viscous organic liquid. The synthetic TiO_2 colloid can be prepared via sol-gel and then hydrothermal growth (Nazeeruddin *et al.*, 1993; Ma *et al.*, 2003; Wang *et al.*, 2003d; Ito *et al.*, 2008). The last one is preparing the paste from synthetic TiO_2 gel via surfactant self-assembly sol-gel, and the TiO_2 gel is blended with commercial TiO_2 powder as binder (Kitiyanan *et al.*, 2005; Ngamsinlapasathian *et al.* 2006; Pavasupree *et al.*, 2006). The two last methods can control the particle size, anatase phase formation, and pore size distribution. Moreover, there are three widely-used film preparation techniques for DSSC: screen printing, doctor blading, and electrophoresis deposition (Kamada *et al.*, 2002; Nguyen *et al.*, 2007). The first technique gives the best results while the last one has been more frequently used to prepare film on plastic substrate for flexible DSSC since it is one promising to avoid the high temperature treatment. The electrodeposition technique will be discussed in section 2.9.

The $TiCl_4$ post treatment is an important procedure of TiO_2 film preparation to improve cell performance. It influences directly to increase inter-particle necking and especially increase the density of specific binding site despite decrease in TiO_2 surface area (Vougioukalakis *et al.*, 2010). It is known that dehydroxylated TiO_2 surface is very active in chemisorption, due to the presence of coordinatively unsaturated Ti^{4+} centers with Lewis acid character as shown in Figure 2.18.

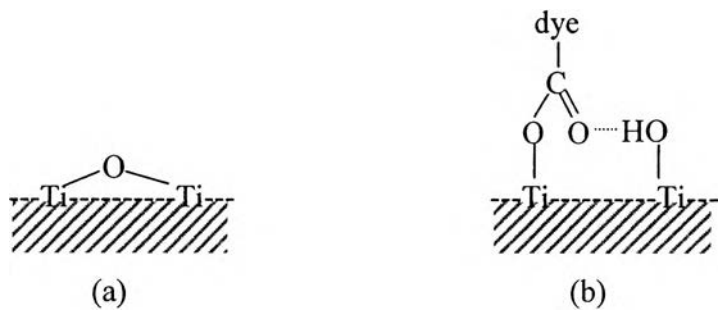

Figure 2.18 Schematics of a) dehydroxylated TiO_2 surface and b) chemisorption of carboxyl group of dye on TiO_2 surface.

On the flat plane surface, oxygen atoms normally hinder the Ti^{4+} and limit the angle of dye adsorption, while the post treatment is supposed to create rough surface with many defects, especially steps and kinks. The less perfect crystal plane or less regular surface will contain highly exposed coordinatively unsaturated Ti^{4+} centers at varying distances, presenting more possibilities for dye adsorption. In addition to higher dye loading in TiO_2 film, this results in more favorable binding angles of the carboxyl attaching groups and hence a strong overlap of the dye π-system with the conduction band of TiO_2, i.e. facilitating electron injection efficiency (Kay, 1994).

Nonetheless, the high surface area and lots of defects on the surface would cause a number of surface states or trap states as shown in Figure 2.19 (Frank *et al.*, 2004; Kopidakis *et al.*, 2006; Ofir *et al.*, 2006; van der Lagemaat et al., 2000), resulting in high electron recombination at bare TiO_2 surface, which contacts directly to the electron acceptor or triiodide in the electrolyte. In fact, the bare surface of TiO_2 comes from (i) the surface within nanopore where macromolecules of dyes cannot penetrate to adsorb, (ii) low dye coverage, (iii) low basic species coverage (such some additives in electrolyte), and (iv) high ionic strength which decreases potential of electron donor species adsorbing on TiO_2.

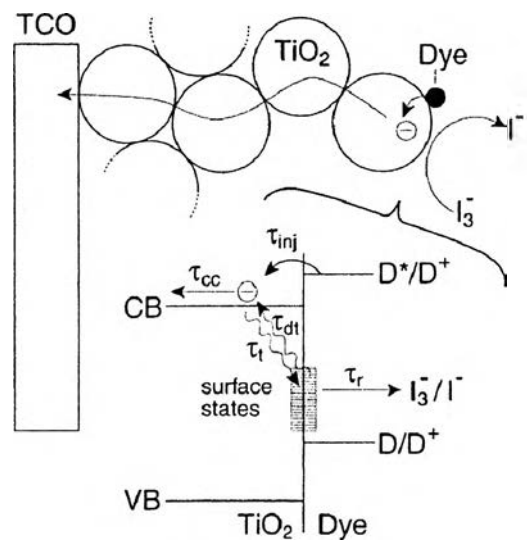

Figure 2.19 Scheme showing the important kinetic parameters with surface states (van der Lagemaat et al., 2000).

Since "A major photovoltage loss mechanism is the disappearance of photoelectron density in the film due to recombination at the TiO_2/electrolyte interface" (Kopidakis *et al.*, 2006), one method to reduce the interfacial recombination losses by triiodie scaventure due to the bare surface of TiO_2 is coating of semiconductor oxides with a thin overcoat of another metal oxide with a higher conduction band edge as a core-shell barrier, such as ZnO, Nb_2O_5, SrO, and $SrTiO_3$. Moreover, the nanometer overcoat of insulating barrier, such as $CaCO_3$, MgO, Al_2O_3, ZrO_2, and SiO_2 was also introduced by Kong *et al.* (2007). Since the higher conduction band edge of these metal oxide acts as an insulator between injected electron and triiodide, the electron density of conduction band of TiO_2 increases, affecting to the improvement of open-circuit voltage. However, some of them suppressed much the photocurrent density while they renders very high open-circuit voltage and fill factor. This resulted in reducing the overall performance of the solar cells (Kay and Grätzel, 2002).

Even though the barrier is not completely overcoated on semiconductor, it is still effective. Nguyen *et al.* (2007) employed the SiO_2 particles as an energy barrier by using electodeposition method to prepare the film. The electrostatical attractions between TiO_2 and SiO_2 nanoparticles formed a titania–silica complex, $[(SiO_2)_x(TiO_2)_n]^{(n-x)+}$, which has the intimate contacts between them in comparison with doctor-blading method. This can decrease recombination and increase photovoltaic properties.

2.5.3 Electrolytes and Hole Conductors

The electron accepters or hole-conducting media classifies DSSC into three types, which are liquid-state DSSC, solid-state DSSC and quasi-solid-state DSSC.

2.5.3.1 Liquid-State DSSC

Normally, the organic liquid is used as solvent, and I^-/I_3^- is mostly used as redox couple. The important role of redox electrolyte is regenerating the oxidized dye molecules before recombination or dye aggregation take place. In order to obtain high cell performance and long term cell stability, the redox couple must follow these general requirements (Kay, 1994):

i) The redox couple must have a more negative electrochemical potential than the oxidized dye, so that reduction can take place. It takes around 100 nanosecond for fast dye regeneration via reduction by I^- without voltage bias (Haque *et al.*, 1998).

ii) The redox potential should be as positive as possible to provide large open circuit voltage.

iii) The redox couple must be reversible at the counter electrode but not on the TiO_2 electrode.

iv) The electrolyte must not absorb strongly in the visible spectrum.

v) The electrolyte should not quench the excited state of the sensitizer, in particular too high concentration of the oxidized form of the redox couple.

vi) The electrolyte must be able to carry a current more than 20 mA/cm^2 without diffusion limitation or significant ohmic losses.

vii) To be pratical, the redox electrolyte must be stable on a long term, retain its properties over a fairly wide range of temperatures, but non-toxic, non-volatile and cheap.

The iodide/triiodide redox couple is the most suitable since transferring of electron from TiO_2 to I_3^- is very slow due to the week dissociative chemisorption of the iodine and regeneration of I^- at counter electrode is very fast due to the effective catalytic reaction at the counter electrode (Lee *et al.*, 2011). On the other hand, other redox couples like $SCN^-/(SCN)_2$ (Oskam *et al.*, 2001) , $SeCN^-/(SeCN)_2$ (Oskam *et al.*, 2001), ferrocene/ferricinium (Fc/Fc^+) (Daeneke *et al.*, 2011) and Co^{2+}/Co^{3+} complex (Nusbaumer *et al*, 2001; Sapp *et al.*, 2002; Nusbaumer *et al.*, 2003; Wang *et al.*, 2010; Tsao *et al.*, 2011) render the fast reaction of electron in TiO_2 and oxidized mediator. Meanwhile, Br^-/Br_2 provided unstable cell because the strongly oxidized Br_2 is too reactive (Kay, 1994) and dye desorption occurrence was reported by Hara *et al.* (2001). Among these high redox potential compared to that of I^-/I_3^-, it seems that polypyridyl Co^{2+}/Co^{3+} complex is the most popular since it provided excellent cell performance at low light intensity but it suffers at full sunlight as mass transfer limitation due to its bulky molecule. Recently, Tsao *et al.*

(2011) reported the highest DSSC efficiency of cell with cobalt based electrolyte at 9.6% under full sunlight by tuning the TiO_2 film thickness and cobalt complex concentration, and they also found that besides the improvement of V_{oc} due to its high redox potential (0.49 V vs NHE compared to 0.31 V vs NHE of iodide redox potential) and the lower light absorption of cobalt based electrolyte than that of the iodide based electrolyte in the range of 400-450 nm, the red shift of IPCE spectrum starting at around 600 nm was the main contribution to arise the J_{sc} of cell with cobalt based electrolyte over that of iodide based.

The counterions of reductive redox species are also greatly affect the cell performance. The increase in the adsorption cation species on TiO_2 surface , which depends on the decrease in cation radius causes the potential drop in the Helmholtz layer (Hara *et al.*, 2001) or more positive acceptor levels in TiO_2 (Kay, 1994). This would be shifted the conduction band level of TiO_2 positively and results in an increase in the driving force for the electron injection process from the LUMO of dye molecule into conduction band of TiO_2, leading to an increase in current while a decrease in voltage. The most effective cation with the smallest radius is Li^+ as reported by Liu *et al.* (1998). Interestingly, the presence of lithium ions was found to accelerate the dye regeneration by iodide, which was attributed to electrostatic interactions (Tachibana *et al.*, 2001; Wang *et al.*, 2003a; Zakeeruddin and Grätzel, 2009).

The addition of additives in an electrolyte is plays an important role to enhance the cell performances. The adsorption of basic species like pyridine derivatives on the surface shifts the conduction band of photoanode negatively along with suppression of the dark current by blocking surface state, consequently decreasing the reduction rate of I_3^-, resulting in increasing the V_{oc} and fill factor (Nazeeruddin *et al.*, 1993; Kong *et al.*, 2007). For example, the employed base species are *ter*-butylpyridine (Nazeeruddin *et al.*, 1993), N-methyl benzimidazole (NMBI or NMB) (Kong *et al.*, 2007; Zakeeruddin and Grätzel, 2009; Wang, 2009), and N-butylbenzimidazole (NBB) (Kung *et al.*, 2007; Bai *et al.*, 2008, Zakeeruddin and Grätzel, 2009). Meanwhile, guanidine thiocyanate (GuNCS) (Lee *et al.*, 2007; Gao *et al.*, 2008) with its guanidine cation adsorbing on TiO_2 surface slows recombination by 1 order of magnitude. Even it also induces a downward shift of the

TiO_2 conduction band edge, the net effect was an improved V_{oc} (Kopidakis *et al.*, 2006). The molecular structure of these species is depicted in Figure 2.20.

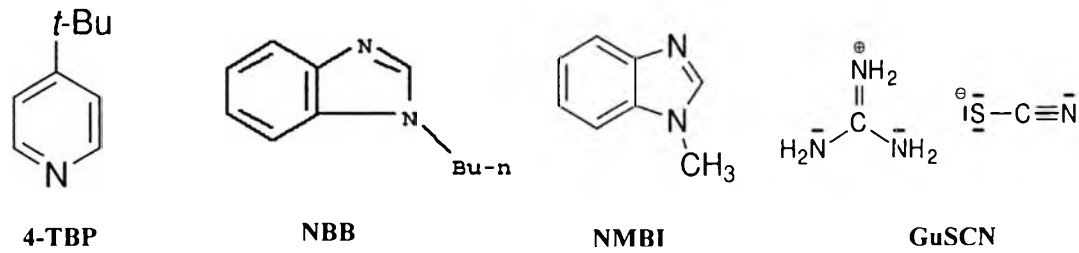

4-TBP **NBB** **NMBI** **GuSCN**

Figure 2.20 The molecular structure of additives in electrolyte.

Different organic solvents influence the cell performance in different ways. Hara *et al.* (2001) reported that larger photocurrent densities were obtained in nitrile solvents but larger V_{oc} was obtained in basic solvent or high donor number solvent such as dimethylsulfoxide (DMSO), N,N-dimethylformamide (DMF) and N-methyl-2-pyrolidone (NMP). These are attributed to high dielectric constant of nitrile solvents to contribute the ion pair dissociation and negative shift in the conduction band of TiO_2 due to adsorption of basic solvent, respectively. However, the basic property of solvent results in dye desorption which was not observed in nitrile solvents (Hara *et al.*, 2001). In alcoholic solvents such as methanol and ethanol was also obtained large V_{oc} but caused unstable cell owing to dye desorption (Hara *et al.*, 2001).

Besides, the high viscosity solvent results in a poor diffusion of the redox couple and causes the reduction of the current, as well as the fill factor, which depends on series resistance in the DSSC (Hagfeldt *et al.*, 1994). Concentration of redox couple, however, must not be too high; high concentration may increase the viscosity of the solution and reduce V_{oc} due to an increase in I_3^- electron scavengers, which enhance the back electron transfer reaction (Hara *et al.*, 2001; Kebede *et al.*, 1999).

DSSCs based on these liquid electrolytes provide the highest efficient cells at the present as their low viscosity properties lead to high charge mobility. However, the leakage is a very serious problem, which causes cell stability,

in particular volatile substances. We can also define this liquid-state DSSC according to physical property of liquid electrolyte. Those are volatile electrolyte, low-volatile electrolyte, and solvent-free or ionic liquid electrolyte. As we known, acetonitrile-based electrolyte renders the high efficient cell but itself is high volatile solvent. To prolong the cell life time, the mixtures of high boiling point solvents with acetonitrile are used. The high boiling point solvents such as 3-methoxy propionitrile (MPN) is employed as low-volatile solvent even though their high viscosity diminished the cell performance. However, the evaporation process still occurs. It seems the ionic liquid is the best solution because it is a molten salt at room temperature (RTIL) and non-volatile substance. In addition, low viscosity of the molten salt (Bai *et al.*, 2008; Cao *et al.*, 2008; Gao *et al.*, 2008) has been found and this improves cell performance almost as good as that of cell with low-volatile electrolyte.

Since the viscosity is a main key to succeed high cell performance, the binary system of ionic liquid iodide salts and other ionic liquid salts which have lower viscosity were employed, for example the mixture of 1-propyl-3-methylimidazolium iodide (PMII) with other salts like 1-methyl-3-ethylimidazolium dicyanamides (EMIDCN) (Wang *et al.*, 2003a), 1-ethyl-3-methylimidazolium thiocyanate (EMINCS) (Wang *et al.*, 2004b), 1-ethyl-3-methylimidazolium tricyanomethanide (EMITCM) (Wang *et al.*, 2005) or etc. In 2008, Cao *et al.* reported a new low viscosity ionic liquid electrolyte of eutectic melt-based ILs. This system combined of solid ionic liquids at room temperature of 1,3-dimethylimidazoliumiodide (DMII), 1-ethyl-3-methylimidazolium iodide (EMII) and 1-allyl-3-methylimidazolium iodide (AMII) to obtain RTIL with high conductivity and low viscosity. The viscosity decrease in order RTIL of 1-hexyl-3-methylimidazoulium iodide (HMII) > 1-butyl-3-methylimidazolium iodide (BMII) > PMII > eutectic melt based IL of DMII/EMII/AMII, and the molar concentration of iodide melts in HMII < BMII < PMII < DMII/EMII/AMII which is in the converse order with molar volume of system. Besides the viscosity, the conductivity increases with iodide density or molar concentration of iodide melt. In addition, the replace of AMII with low viscosity RTILs like 1-ethyl-3-methylimidazolium tetracyanoborate (EMITCB) (Bai *et al.*, 2008) or EMINCS (Cao *et al.*, 2008) provided more efficient ionic liquid electrolyte.

Nevertheless, the conductivity of ionic liquid electrolyte does not directly relate to the viscosity as Einstein-Stokes theory. Zistler *et al.* (2006) found that the diffusion coefficient of triiodide decreased only 30% while the viscosity of binary ionic liquid electrolyte containing PMII and $BMIBF_4$ mixtures increased by 1,000%. "This was explained by the Grotthus-type exchange mechanism enhance the diffusion process at higher concentration of iodide. The triiodide approaches iodide from one end, forming an encounter complex, from which triiodide is released at the other end. In this fashion, the triiodide is displaced by the length of one I–I bond, i.e., 2.9 Å, without having to cross that distance. The bond exchange occurs immediately upon formation of the encounter complex, rendering the process diffusion-controlled. Thus, the viscosity-dependent transport of triiodide in IL electrolytes with high iodide concentration can be described by physical diffusion coupled to the Grotthus bond exchange." (Zakeeruddin and Grätzel, 2009)

To overcome the several drawbacks of iodide/triiodide redox couple for instance V_{oc} limitation, corrosion and strong visible light absorption, other redox couples have been discovered. Free-iodide-based ionic liquid electrolyte containing $SeCN^-/(SeCN)_3$ redox couple provided higher efficient DSSC than that of iodide-based ionic liquid electrolyte since it exhibits good resistance for recombination reaction at TiO_2, and rather high conductivity and low light absorption in visible range (Wang *et al.*, 2004c). However, it rendered unstable DSSC under the thermal and light-soaking dual stress (Cao *et al.*, 2008). Other Free-iodide-based ionic liquid electrolytes have performed low efficient DSSC.

2.5.3.2 Solid-State DSSC

Recently, many attempts have been made to solve the liquid-state DSSC problems by the replacement of liquid electrolyte with hole transport materials (HTM). The hole transport materials employed in solid-state DSSCs can be classified as p-type semiconductors and polymer electrolytes which is solvent free or pure polymer electrolyte. The inorganic p-type semiconductors used in solid-state DSSC are, for example, CuI (Kumara *et al.*, 2006; Tennakone *et al.*; 1995) or CuSCN (O'Regan and Schwarz, 1998). Even their efficiencies has been quite low

due to low contact between dye molecules in highly porous TiO_2 and hole conductor (Grätzel, 2001), the maximum efficiency of cell with CuI and EMINCS as crystal growth inhibitor was 3.8%. The organic p-type semiconductors are conductive polymer, polymer electrolyte, and organic molecule. The conductive polymers are, for example, polyaniline, polypyrrol, and polythiophien (Nogueira *et al.*, 2004). The polymer electrolytes are composed of alkaline salts (e.g. lithium or sodium salts) dissolved in a high molar mass polyether host (e.g. poly(ethylene oxide) (PEO) or poly(propylene oxide) (PPO)) (Armand, 1987). The solubility of the salt depends on the ability of the electron donor atoms in the polymer chain to coordinate the cation through a Lewis type acid–base interaction. Spiro-OMeTAD (Figure 2.21), the organic molecule is the most promising one since the maximum cell performances reported by Cai *et al.*, (2011) was Jsc = 9.74 mA/cm^2, Voc = 0.88V, ff = 0.71, and η = 6.08%. This achievement employed the organic dye, C220 and 2 μm thickness of TiO_2 film. Cai *et al.* (2011) mentioned that the incomplete pore filling of thicker TiO_2 films with solid HTMs restricted the solid-state DSSCs to using thinner TiO_2 films with high molar extinction coefficient dyes. As a result, solid HTMs have shorter charge carrier diffusion lengths than liquid redox electrolytes.

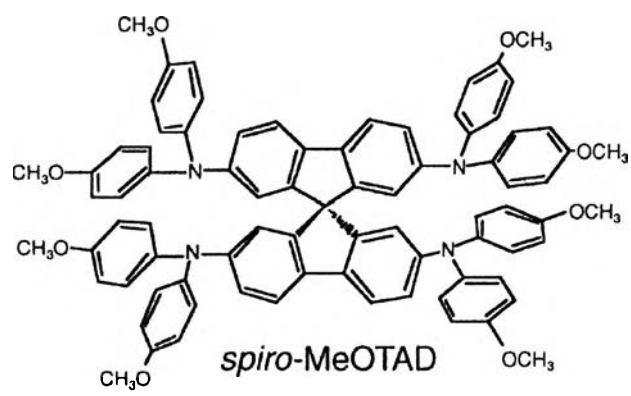

Figure 2.21 The chemical structure of spiro-OMeTAD (Grätzel, 2005).

2.5.3.3 Quasi Solid-State DSSC

Since liquid-state DSSCs have the sealing problem and difficultly fabricate along with solid-state DSSCs obtains low efficient DSSC, the

quasi solid-state DSSC would be the solution to compromise the advantages and drawbacks of both former DSSCs. Quasi-solid state or gel electrolyte prolongs the cell life time under light soaking more efficient than liquid electrolyte does. Besides, the solid-like property contributes the use of manufacturing technique as screen printing or blading. Currently, high efficient DSSC with gel electrolyte could reach 10% with acetonitrile as a solvent (Inoue *et al.*, 2010). Nevertheless, the gel electrolyte with this kind of solvent still faced the sealing problem as its very low boiling point which also made cell poor stability. Therefore, high boiling point solvent such as MPN or RTILs could be more practical. As a gel composes of solvent and gelator, discovering the good compatible gelator with acetonitrile to retard the evaporation process would be challenge. Normally, the gelators are polymer, nano-metal oxide, or nanocomposite of nano-metal oxide and polymer. There are several kinds of polymer used to gel liquid electrolyte depending on donor number and dielectric constant of each polymer as those factors influence the polymer-solvent compatibility (Wu *et al.*, 2007) and the ion dissociation (Wang *et al.*, 2004e). In contrast with Li battery, donor number affects much the conduction band movement of TiO_2 than the ion dissociation since the larger V_{oc} is always obtained while the smaller J_{sc} takes place (Wu *et al.*, 2007). The dielectric constant is the important factor for ion pair dissociation, which leads to increasing J_{sc} of the cells (Wu *et al.*, 2007). However, matching of donor number and dielectric constant of polymer and solvent is very important as a polymer could be gelled or swollen in a group of solvent. The compatible should be enough to cage solvent inside polymer structure, and the interaction between polymer and solvent should be higher than that of between polymer chains in order to generate a great ion transportation channels (Wang *et al.*, 2009) and enhance cell stability (Pasquier, 2007). On the contrary, the viscosity of medium also increases with the strong interaction between polymer and solvent, rendering low triiodide diffusion coefficient (Pasquier, 2007). As mentioned above, different kinds of polymer were used according to the kind of solvent. For example, high donor number solvents like propylene carbonate, ethylene carbonate, diethyl carbonate, N-methyl pyrrolidone, γ-butyrolactone or their mixture are favorably used with polyethylene oxide (PEO), polyacrylamide (PAM), copolymer of PEO and PAM (Wu *et al.*, 2006), PEO and polyacrylic acid (PAA)

(Wu *et al.*, 2007) or polyvinylidenefloride-co-hexafluoropropylene (PVDF-HFP) (Pasquier, 2007). This group of gel electrolyte provided quite low DSSC efficiency because of their low dielectric constant and high viscosity of solvent. Another class of gel electrolyte consists of high dielectric constant solvent such as acetonitrile and MPN. This kind of electrolyte incorporating with medium dielectric constant polymer like polyacrylonitrile (PAN), polymethyl methacrylate (PMMA) or PVDF-HFP, endowed more cell performance compared to the previous group. In particular, the efficiency of cell with PVDF-HFP could be comparable with that of liquid-state DSSC (Wang *et al.*, 2004d) and even higher than that of cell with liquid electrolyte such in the study of Li *et al.* (2007). They used poly(vinylpyridine-co-acrylonitrile) (P(VP-co-AN)) as gelator for liquid electrolyte and then V_{oc} of the cell was improved. As a result, polyvinylpiridine (PVP) contains the same part with TBP, an additive in electrolyte for DSSC. The chemical structure of P(VP-co-AN) is shown in Figure 2.22.

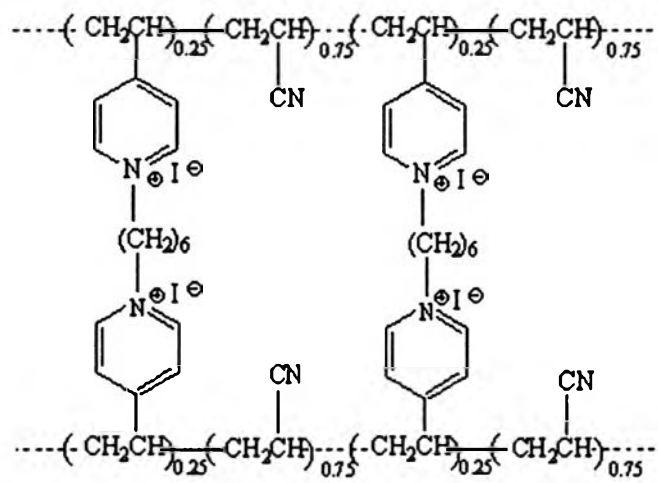

Figure 2.22 The chemical structure of P(VP-co-AN) (Li *et al.*, 2007).

Even most of polymer gel electrolytes provide relatively low DSSC performances, some nano-metal oxide addition or nanocomposite gel could enhance the cell efficiency such as the incorporation of montmorillonite (MMT) with poly (n-isopropylacrylamide) (PNIPAAm) (Tu *et al.*, 2008), MMT (Lai *et al.*, 2009) or mica (Lai *et al.*, 2010) with PVDF-HFP, and TiO_2 or graphite with PVDF-HFP

(Huo *et al.*, 2007; Lee *et al.*, 2008a). The improvement was the increase in J_{sc}, attributed to the contribution of Grotthus-type exchange mechanism and light adsorption improvement in wavelength of 400-550 nm (Tu *et al.*, 2008; Park *et al.*, 2008; Lai *et al.*, 2009; Lai *et al.*, 2010).

Unsurprisingly, nano-metal oxide gel electrolyte exhibited as high cell performance as liquid-state DSSC did such as fumed silica (Wang *et al.*, 2003e; Wang *et al.*, 2004d). In addition, the nano-metal oxide gel electrolyte of aluminosilicate oxide such clay could enhance the cell performance over that of liquid-state DSSC (Park *et al.*, 2008; Inoue *et al.*, 2010). It was observed that the ion diffusion coefficient of triiodide in gel electrolyte was higher than that in liquid one (Inoue *et al.*, 2010).

2.5.4 Counter Electrode

Solar cell studies employ usually F-doped SnO_2 as the conducting glass electrodes. Such electrodes are known to be poor choice for efficient reduction of triiodide. To reduce the overvoltage losses, a very fine Pt-layer or islands of Pt is deposited onto the conducting glass electrodes. This ensures high exchange current densities at the counter-electrode, and thus the processes at the counter electrode do not become rate limiting steps in the light energy harvesting process. Besides Pt, the other alternative materials can be gold or graphite.

2.6 Co-Adsorbates of Phtosensitizers

There have been several kinds of co-adsorbates used widely to improve performances of the DSSC, such as cholic acid (Kay and Grätzel, 1993), deoxycholic acid (Lee *et al.*, 2007) (Figure 2.17), hexadecylmalonic acid (HDMA) (Wang *et al.*, 2003d), 3-phenylpropionic acid (PPA) (Wang *et al.*, 2004b), 1-decylphosphonic acid (DPA) (Wang *et al.*, 2003c), 4-guanidinobutyric acid (GBA) (Zhang *et al.*, 2005) and etc. The chemical structures of co-adsorbates are shown in Figure 2.23. The co-adsorbate and dye molecules will result in the formation of mixed monolayer, which should be more tightly packed than when the dye is adsorbed alone, providing a more effective insulated barrier for the back electron transfer from TiO_2 conduction band

to triiodide electrolyte by hydrophobic spacer effect (Kopidakis et al., 2006; Lee *et al.*, 2007). As a result, this produces the high V_{oc} while the photocurrent increases as the co-adsorbate reduces the dye aggregation either by suppressing the quenching processes of the energy transfer or shifting the conduction band edge of the TiO_2 positively (Lee *et al.*, 2007). In addition, co-adsorbates could enhance thermal stability which is usually influenced by the photovoltage reduction owing to the photo-induced proton intercalation on TiO_2 surface during the light soaking process (Chen *et al.*, 2009a; Chen *et al.*, 2009b). For instance, the long alkyl chain of alkylphosphonic acid like DPA excludes the water from the interface of TiO_2/dye (Wang *et al.*, 2003c).

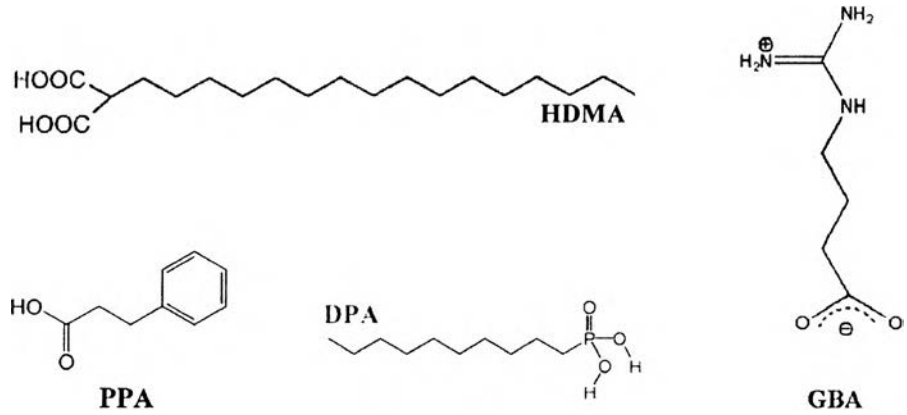

Figure 2.23 The chemical structures of co-adsorbates.

2.7 Sol-Gel

Sol-gel method is a chemical route to synthesis of a colloid suspension of ceramic particles (sol) in liquid media and subsequently to formation of particle network filled with a solvent (wet gel). The wet gel converts to a xerogel when it dried at ambient pressure, and converts to aerogel when it dried at supercritical condition. (faculty.washington.edu/gzcao/group/solgel.htm.)

Sol is prepared first from the precursors (either organic or inorganic). Two chemical reactions following 2.8 and 2.9 eq. are involved: hydrolysis and condensation with acid or base as catalyst. (faculty.washington.edu/gzcao/group/solgel.htm.; Otterstedt and Brandreth, 1998)

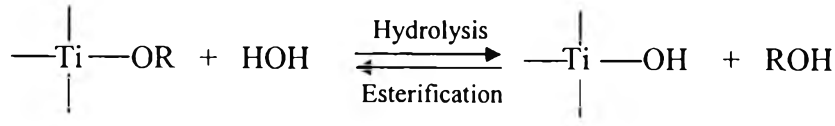

(2.8)

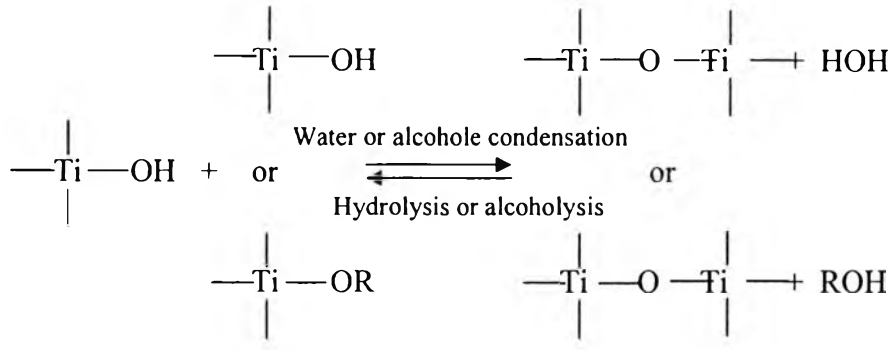

(2.9)

Sol particle is around 1-1000 nm which is small enough to be stabilized by an electric double layer, or steric repulsion, or their combination. Sol-gel allows materials to be mixed at atomic level, and allows solid particles and/or crystallization and densification to form at low temperature including. (faculty.washington.edu/gzcao/group/solgel.htm.)

There are several factors that affect the rate reactions, particle size, particle size distribution, crystallization, and etc. Usually, hydrolysis and condensation reactions of metal inorganic and small metal alkoxide occur very rapidly, resulting in less uniform and large particle size. Use of the bulky branched alkoxy groups (such as isopropoxides) reduces the hydrolysis and condensation rate, leading to the formation of small colloidal clusters and a more uniform particle size (Wang and Ying, 1999).

High H_2O/metal molar ratio increased the hydrolysis rate and it could complete hydrolysis reaction before condensation starts when the ratio reached an optimal point. (Corsi.chem.polimi.it) Moreover, the high hydrolysis rate favored nucleation versus particle growth, leading to reduce crystallite size (Mahshid *et al.*, 2007; Wang and Ying, 1999). Wang and Ying (1999) found that anatase nanocrystals of 20 nm could be obtained by calcining titania gel synthesized with a water: alkoxide ratio of 165. Likewise, the high water/ethanol ratio in mixed solvent allowed more complete hydrolysis reaction to promote nucleation of nanocrystals

(Otterstedt and Brandreth, 1998; Wang and Ying, 1999). Besides, high amount of water increased the degree of crystallization at lower temperature whereby particle growth was minimal so the high crystalline with small grain size could occur (Mahshid *et al.*, 2007; Wang and Ying, 1999). However, this also lowered anatase to rutile formation temperature of TiO_2 due to the high surface energy of the particles (Mahshid *et al.*, 2007).

Wang and Ying (1999) mentioned that addition of acid or base catalysts controlled the sol-gel reaction rate. Even though the presence of HCl flavored both hydrolysis and condensation reaction (Del Castillo *et al.*, 1997), they found that the presence of acid catalyst promoted the hydrolysis reaction versus the condensation reaction, causing the reduction of crystallite size from 20 nm to 14 nm when HCl at HCl: alkoxide molar ratio of 0.25 was added in the reaction medium for the system with water: alkoxide ratio of 165 and calcinations temperature at 450 °C. This is in accordance with the report of Del Castillo *et al.* (1997) that the pH higher than 1.5 was necessary for polymerization of titanium polycation. Beside acid preventing the particle growth, it served as an electrolyte to prevent agglomeration or flocculation of the TiO_2 sol at high water content through electrostatic repulsion (Wang and Ying, 1999, LaCourse and Kim, 1986). Nevertheless, the zero point of charge (ZPC) of TiO_2 is near pH 6. Thus, ionization of hydrolyzed bonds on either side of the ZPC would also result in deflocculation of the sol. However, gel could formed under either acid or base condition but acid catalyze sols may required longer time for gelation and the gel trend to be weak (LaCourse and Kim, 1986).

2.8 Light Scattering

As it has already known that the absorption path length can increase by increasing of TiO_2 film thickness but in thicker cell, the series resistance grows rapidly with path lengths of the electrons and redox couple species (Ferber and Luther, 1998). Therefore, in liquid DSSCs, the optimal electrode thickness is in the range of 10-15 μm (Ferber and Luther, 1998) and it is quite low especially in solid state one. Besides the high molar extinction coefficient dye, scattering layer or center increases light absorption path length more effective than increase in active

transparent layer since high photocurrent density of DSSC could be obtained in thinner films, in which charge recombination can be reduced due to a lower film resistance (Hore *et al.*, 2006; Usami, 2000). Moreover, light absorption of dye molecules remains poor in particular in the wavelength of 600-800 nm, but light scattering in the TiO_2 electrode can also increase more the path length of the incident radiation and therefore enhance the absorption in red-light region (Ferber and Luther, 1998). In addition, with light scattering phenomenon, thinner sensitized films could reduce the amount of expensive synthetic dyes without decrease the amount of light absorbed by the dye molecules. Then, this is a way to lower cost of DSSCs (Hore *et al.*, 2006).

Light scattering can be took place with a change in the refractive index between the active layer of TiO_2 and the scattering layer on the top of active layer, and the ability of this scattering layer depends on the relative size of the particles in the layer (Hore *et al.*, 2006). Two main scattering theories are applied from Mie theory, which is effective to spherical particle size in the range or comparable to the light wavelength (Hore *et al.*, 2006; Ferber and Luther, 1998), and Rayleigh theory, which corresponds to the particle size much smaller than the wavelength and it is stronger effective to shorter wavelength (en.wikipedia.org/wiki/Rayleigh_scattering). Thus, to enhance red-light absorption the Mie theory must be applied. Nevertheless, large TiO_2 particle with size in the range of about 100-1,000 nm and other higher refractive index materials (Hore *et al.*, 2006) can be used as light scattering centers. Besides some other inactive particles in spherical shape (Hore *et al.*, 2006), flakes (Yasuda *et al.*, 2010) have also been used as scattering layers or reflectors on the top of active layer effectively. Furthermore, the admixed particle of different particle sizes is also effective (Ferber and Luther, 1998; Wang *et al.*, 2004a; Usami, 2000), but the volume fraction of the scattering particles should not excess about 10-30% because of lower surface area for dye adsorption (Ferber and Luther, 1998; Usami, 2000) and too much back scattering which rather enhanced the cell reflectance than the cell absorbance (Ferber and Luther, 1998). Rothenberger *et al.* (1999) found that the photoactive layer of TiO_2, containing 65% and 35% by weight of transparent and scattering colloids, provided the maximum light conversion to electric, especially in red-light region. In addition, the admixing of spherical voids (Hore *et al.*, 2005) in

the TiO_2 layer can enhance light scattering via different in the refractive index of nanocrystalline TiO_2 film and electrolyte. Moreover, it is useful for electrolyte and hole conductor materials to contribute their penetration into the porous TiO_2 and improve ion transportation, consequently improving overall DSSC performance.

2.9 Natural Clay: Na-Bentonite and Its Intercalation

Na-bentonite is one type of clay, an aluminium phyllosilicate, which is mainly composed of montmorillonite and has Na ion as dominant cation. Its particle size is less than two micrometers and its gap between particles expands when it wets, possibly absorbing water several times of its dry mass.

Montmorillonite, a member of the smectite family, is a 2:1 clay, meaning that it has 2 tetrahedral sheets sandwiching a central octahedral sheet in one platelet. Its structure is shown in Figure 2.24. "The sum of a single layer (~1 nm) plus the inter layer represents the repeat unit of multilayer and is calculated from the 001 harmonies obtained from X-ray diffraction pattern" (Giannelis et al., 1992). One repeat unit of montmorillonite is around 12-14 Å (Lee and Lee, 2004; Moraru, 2001; Tyagi *et al.*, 2006). There is an unsatisfied negative charge on the face of the clay platelet caused by structural substitutions or vacancies in the octahedral and/or tetrahedral layers. For example, Mg^{2+} or another divalent cation may substitute for Al^{3+} in the octahedral layer, or Al^{3+} or Fe^{3+} may replace Si^{4+} in the tetrahedral layer. Inorganic cations, such as Ca^{2+}, Mg^{2+}, and Na^{+}, are attracted to the spaces between the platelet due to the net negative charge on the "faces" of the platelet. Water is adsorbed between these platelets. These cations can be exchanged readily through washing. Chemically, Montmorillonite is identified as hydrated sodium calcium aluminium magnesium silicate hydroxide $(Na,Ca)_{0.33}(Al,Mg)_2(Si_4O_{10})(OH)_2 \cdot nH_2O$ (www.origins.rpi.edu/claycatalyzed.html.) and classified different from other phyllosilicates according to the localization and abundance of crystalline lattice substitutions as shown in table 2.3.

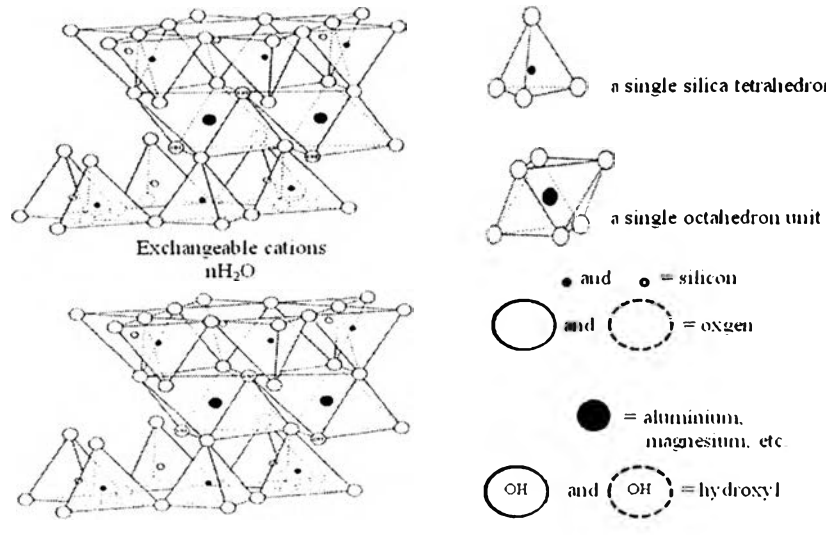

Figure 2.24 Montmorillonite structure.

The swelling of silicates can intercalate a large number of polar molecules in their galleries with a substantial increase in the gallery height via ion exchanging (Giannelis *et al.*, 1992). These polar molecules would balance the charge deficiency in the layers (Giannelis *et al.*,1992). The intercalation of guest species into the host galleries is facilitated by the much weaker interlayer forces compared to those in the layer (Giannelis *et al.*, 1992; Kanamaru, 1988). In addition, Intercalated structure is a starting form of nanoclay since the intercalation of any guest species would extend more the distance between silicate layers, which could observed from the shift of 001 peak from XRD pattern to smaller angles as shown in Figure. 2.25, and also is a host for producing nanostructure with high porous and surface area. The examples of these intercalated clays with various guest species are organoclays with quaternary ammoniums bearing long alkyl chains (Lee and Lee, 2004; Moraru, 2001; Muksing *et al.*, 2008; Önal and Sarıkaya, 2008; Picard *et al.*, 2007) (Figure. 2.26a), pillared clays with metal oxides (Damardji *et al.*, 2009; Del Castillo *et al.*, 1997; Liu *et al.*, 2006; Molinard *et al.*, 1994; Valverde *et al.*, 2002) (Figure. 2.26b), porous clay heterostructures with metal oxides and surfactant templates (Galarneau *et al.*, 1995; Pires *et al.*, 2004) (Figure. 2.26c). The applications of these nanoclays and nanostructures are nanocomposites, catalysts, absorbents, sensor, and etc.

Table 2.3 Classification of phyllosilicates according to the localization and abundance of crystalline lattice substitutions (Duc *et al.*, 2005)

Charge (x) moles per half unit cell	Dioctahedral	Trioctahedral
1:1 Sheet	Kaolinite	Serpentine
0	$Al_2Si_2(O_5)(OH)_4$	$Mg_3Si_2(O_5)(OH)_4$
2:1 Sheet	Pyrophyllite	Talc
0	$Al_2Si_4(O_{10})(OH)_2$	$Mg_3Si_4(O_{10})(OH)_2$
Smectites	Octahedral substitutions	
	Montmorillonite	Hectorite
0.2–0.6	$(Al_{2-x}Mg_x)Si_4(O_{10})(OH)_2(CEC)_x$	$(Mg_{3-x}Li_x)Si_4(O_{10})(OH)_2(CEC)_x$
	Tetrahedral substitutions	
	Beidellite	Saponite
	$Al_2(Si_{4-x}Al_x)(O)_{10}(OH)_2(CEC)_x$	$Mg_3(Si_{4-x}Al_x)(O_{10})(OH)_2(CEC)_x$
Micas	Illite	Vermiculite
0.6–0.9	$(Al_{1.75}R_x)Si_{3.5}Al_{0.5}(O_{10})(OH)_2K_{0.75}$	$(MgFe_3)(Si_{4-x}Al_x)(O_{10})(OH)_2Mg_x$
	Glauconite	Phlogopite
1	$(Al_{2-x}Fe^{3+}Fe^{2+}Mg)(Si_{3.75}Al_{0.25})(O_{10})(OH)_2K$	$Mg_3(Si_3Al)(O_{10})(OH)_2(K)$
	Muscovite	Biotite
	$Al_2(Si_3Al)(O_{10})(OH)_2K$	$(Mg.Fe^{2+})_3(Si_3Al)(O_{10})(OH)_2(K)$

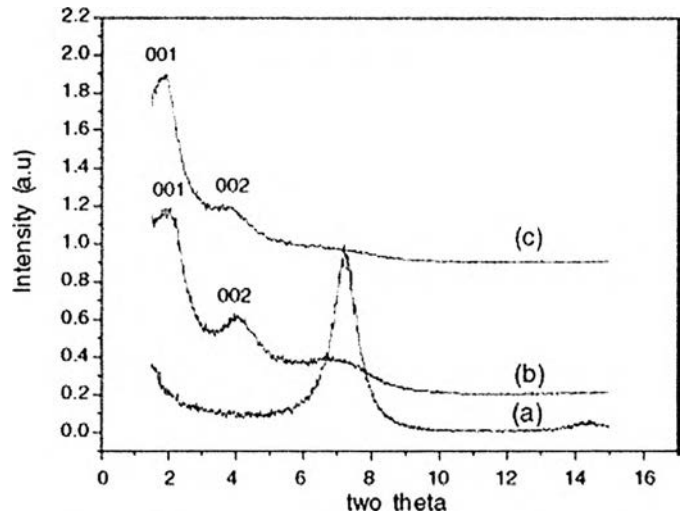

Figure 2.25 Powder X-ray diffraction pattern for (a) montmorillonite, (b) pillared montmorillonite, and (c) iron-doped pillared montmorillonite (Liu *et al.*, 2006).

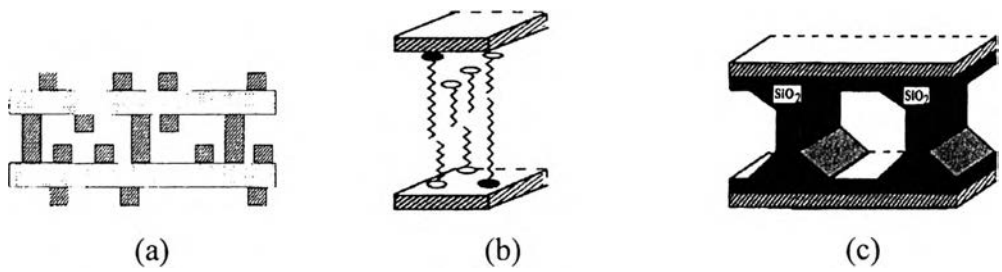

Figure 2.26 a) pillared clay (Molinard *et al.*, 1994), b) organoclay (Galarneau *et al.*, 1995), and c) porous clay heterostructure (Galarneau *et al.*, 1995).

Bentonite is an insulator with high aspect ratio. This would contribute the energy barrier function as described in 2.5.2 and according to the study of Nguyen *et al.* (2007). Then, nanoclay and high dispersion of bentonite in composite with semiconductor are the most important factors to enhance the function and improve the DSSC performance.

Organoclay is widely used to form a nanocomposite since its surface was modified to be hydrophobic. This resulted in decreasing of interaction between silicate layers and led to easily delaminate of each layer (exfoliate) when shear force was applied in the mixture system. Another interesting intercalated structure is

pillared clay because it was prepared via the sol-gel synthesis of metal oxide. Thus, this was possibly to obtain pillared clay structure and composite gel for semiconductor electrode simultaneously.

The method to prepare titania pillared clay was not different to the sol-gel process of titania except for the controlling of hydrolysis and condensation rate at proper condition to form an intercalation of titania polycation. Mostly, pH is an important factor to determine size of intercalate and intercalation formation. The presence of titanium polycation ($TiO_x(OH)_{4-2x}$) has been observed when the pH is higher than 1.5 (Del Castillo *et al.*, 1997; Valverde *et al.*, 2002). However, the intercalation was not found at pH higher than 1.8 (Del Castillo *et al.*, 1997). This was ascribed to the presence of the titanium oxide on the external surface (Del Castillo *et al.*, 1997). Del Castillo *et al.* (1997) found that HCl: Ti ethoxide ratio at 2 and the smallest alkoxide provided the maximum amount of intercalation. Liu *et al.* (2006) reported a basal spacing of 46.5 Å at HCl: $TiCl_4$ molar ratio of 6 and calcination temperature of 400 °C while Valverde *et al.* (2002) and Damardji *et al.* (2009) reported a basal spacing of 24 Å at HCl: Ti ethoxide molar ratio of 2.5 and calcination temperature of 500 °C, and a basal spacing of 17.6 Å at HCl: Ti isopropoxide molar ratio of 10 and calcination temperature of 400 °C, respectively.

2.10 Clay Aerogel

As mention in section 2.7, the xerogel is obtained by removing the liquid from the wet gel ("lyogels" or "hydrogels") by heating to a temperature above the boiling point of the liquid at ambient pressure, consequently the gel shrinkage. "The shrinkage of the gel upon removal of the liquid has been attributed to the capillary pull of the receding meniscus in the capillaries of the gel. This interpretation is supported by the observation that shrinkage can be prevented if the liquid is removed under conditions at which no liquid meniscus exists". (van Ophen, 1967) Then, aerogel structure with ultra-low density, high porosity, and low thermal conductivity is obtained. Three methods available under those conditions are a Kistler process (Kistler, 1932), a supercritical CO_2 drying, and a freeze drying.

Freeze drying is an interesting technique to produce clay aerogel since it is conducted at low temperature and more practical to apply in several applications. Freezing the stable clay gel will produce the lamellar structure, whose dimensions are strongly dependent on the temperature of nucleation and freezing rate (Gawryla, 2009). The lamellar structure is therefore a replica of the ice crystal morphology, which grows in the direction from edge toward the center of vial i.e. in the direction of temperature gradient. This is explained by the fact that when an aqueous solution of dispersed particles is frozen, the non-solvent materials or impurities will be excluded from the growing ice crystals and aggregate at the grain boundaries between individual ice crystals. If the interaction between these impurities; for instance, edge to face (EF) conformation of the clay platelets, is strong enough, the final structure will be retained upon the removal or sublimation of ice crystals, as shown in Figures 2.27 and 2.28. (Gawryla, 2009)

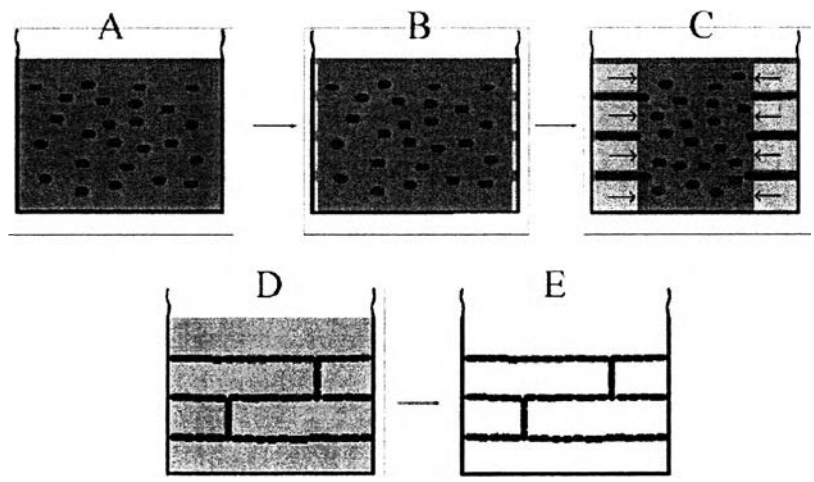

Figure 2.27 (A) stable gel, (B) nucleation at the edge of the vial, (C) ice growth toward the center of vial, (D) frozen solution, (E) after sublimation (Gawryla, 2009).

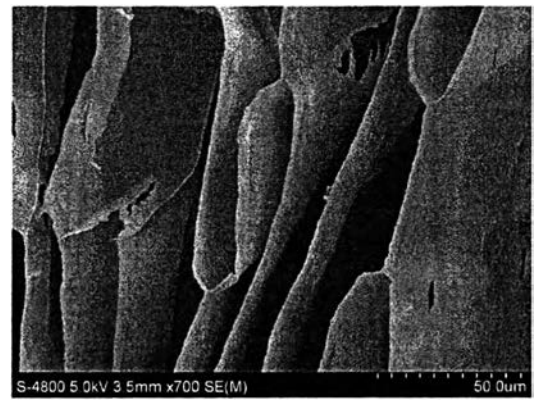

Figure 2.28 FE-SEM micrograph of the clay aerogel.

Regarding this growing of ice crystals, it can be considered that the structures of the aerogels are entirely different from those in the liquid systems (Van Ophen, 1967). "A soft, stacked-layer and highly ordered material was produced, with a sheet-like texture much different from the powdery nature of the starting clays. The starting, macroscopic clay particles of 5-50 μm diameters are comprised of multiple clay sheet aggregates. The clay in these aerogels is not composed of individually exfoliated sheets" (Somlai *et al.*, 2006). Van Ophen (1967) observed a nitrogen surface area of 27 m^2/g, which suggests a particle association of the order of 30 unit layers, corresponded to a thickness of the order of 300 Å. Meanwhile, if the 2-unit-layer-thick clay plates in the hydrogel had remained separated in the aerogel, the nitrogen area of the aerogel would have been of the order of 300-400 m^2/g. The thickness of stack layer and spacing between stacks can be controlled by freezing temperature which involves directly to the speed of ice growing. For instance, by freezing at the temperature of liquid nitrogen, this creates sub-micron to micron thick stack layers with spacing between stack layers in the range of ten to hundred of microns, while freezing at temperatures just below the melting point of water provides the several microns in thickness and millimeter scale spacing. The larger spacing is explained by the fact that each growing crystals have more time to move the impurities out of the crystal growth path (Gawryla, 2009).

Norrish *et al.* (1962) reported intergallery spacings of 18.0 to 20.1 Å for frozen montmorillonite gels and 10 Å for freeze dried materials, indicating the

collapse of the swollen structure with ice crystal formation. Somlai *et al.* (2006) prepared the organically modified clay aerogel and found a increase in montmorillonite (001) spacing from 12.6 to 13.9 Å, denoting the surfactant intercalation.

As the neat clay aerogel is relatively fragile and difficult to handle without damaging its structure, it is therefore important to reinforce the clay aerogel framework with the water-soluble polymers (Bandi and Schiraldi, 2006) to produce the more stable structure. The process can be in situ polymerization and followed by the polymer crosslinking of such PNIPAM (Bandi *et al.*, 2005), or mixing polymer matrix such PVOH (Bandi and Schiraldi, 2006) with the clay aerogel. The relative d-spacing of clay sheet could undergo either a very minor change from 13.9 to 14.3 Å, confirming the absence of extensive intercalation or exfoliation within the composites (Bandi *et al.*, 2005), or a significant change from 13.9 to 15.9 Å, presenting polymer intercalation within the clay platelets in clay aerogel composites (Bandi and Schiraldi, 2006). The clay aerogel structure thus is not completely destroyed even after subjected to high shear and temperature in water; this kinetic stability of clay aerogels in water was recently reported by Somlai *et al.*, 2006. However, the intercalate and exfoliate structures in polymer/clay aerogel composite could achieve via the freeze drying process of well homogenized mixture of polymer latex such natural rubber and swollen clay as described in Pojanavaraphan and Magaraphan's study (2008).

2.11 Electrodeposition

Electrodeposition is an electrochemical method used for the preparation of thin film and coating in wide range of material, such as metals, ceramics, polymers, etc. The advantages of this technique over other coating methods are very uniform coating thickness, high purity, ease for complex fabricated objects, simplicity and economy, and more environmentally friendly. In DSSC application, the electrophoretic technique is one technique which does not need a lot of organic additives (Miyasaka *et al.*, 2002; Miyasaka *et al.*, 2004; Yum *et al.*, 2005), which are burned out at high temperature since only charges and solvent media facilitate the

film formation while screen printing and doctor blading techniques need surfactant and polymer to adjust wet ability and viscosity of the paste.

There are two categories of this technique which are electrophoretic deposition (EPD) and electrolytic deposition (ELD). Electrophoretic deposition is achieved via motion of charged particles toward an electrode under an electric field while electrolytic deposition produces colloidal particles in cathodic or anodic reaction for subsequent deposition (Figure 2.29) (Zhitomirsky, 2002). The main distinguishing features of two methods are that EPD is based on the use of suspensions of charged particles whereas ELD starts from solution of metal salts, and that EPD is an important tool for the preparation of thick film ($\sim 10^{0}$-10^{4} μm) while ELD enables the formation of nanostructured thin films ($\sim 10^{-3}$-10^{1} μm).

We can also divide electrodeposite process into two types: cathodic and anodic processs. In the cathodic process, positively charged material is deposited on the negatively charge electrode, or cathode. In the anodic process, negatively charged material is deposited on the positively charged electrode, or anode. The advantages and disadvantages of both types of processes were described in en.wikipedia.org/wiki/Electrophoretic_deposition. Nevertheless, only cathodic EPD process is going to be emphasized since they related directly to this interested study.

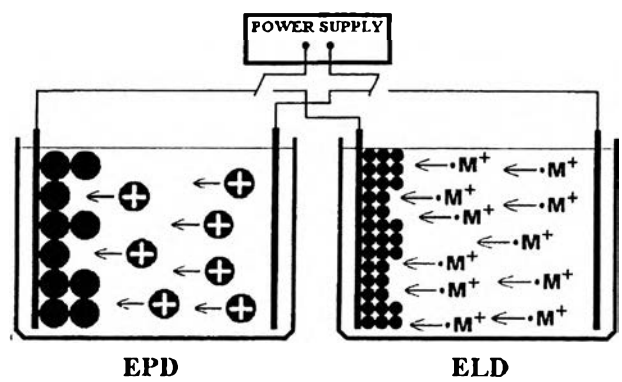

Figure 2.29 Schematic of cathodic electrophoretic deposition (EPD) and electrolytic deposition (ELD) (Zhitomirsky, 2002).

Under an electric field, all of charged species migrate towards the electrode with the opposite charge. The deposit formation is achieved via particle coagulation in front of the electrode and precipitation on the electrode. As the deposited film precipitates, the resistance increases. The increase in resistance is proportional to the thickness of the deposited film, and thus, at a given voltage, the electric current decreases as the film gets thicker until it finally reaches a point where deposition has slowed or stopped occurring (Kaya *et al.*, 2005). This usually occurs in case of constant voltage mode, so to obtain more effective and controllable, the constant current mode is normally introduced (Grinis *et al.*, 2008, Chiu *et al.*, 2011).

Apart from the film formation of charged particles, there are some reactions occurring at the electrodes, particularly the electrolysis of water as shown in the eq. 2.10 and 2.11.

$$\text{Anode: } 2H_2O \rightarrow O_2(\text{gas}) + 4H(+) + 4e(-) \quad (2.10)$$

$$\text{Cathode: } 4H_2O + 4e(-) \rightarrow 4OH(-) + 2H_2(\text{gas}) \quad (2.11)$$

During the aqueous deposition process, gas is being formed at both electrodes. This affects significantly on the coating process. The cathodic process results in considerably more gas being trapped within the film than the anodic process according to the reaction shown above (eq. 2.10 and 2.11). Since the gas has a higher electrical resistance than either depositing film, the amount of gas has a significant effect on the current at a given applied voltage. In addition, the gas formation by the hydrolysis of water which starts above a DC voltage of about 1.4 V results in large pinholes in deposited layers, lack of film uniformity, and poor adherence (Zhitomirsky, 2002; Tabellion *et al.*, 2004). Consequently, solvent used in EPD should be inert with respect to the particles and also originates charges on the colloid particles. The organic solvents such alcohols are the most suitable choice since they behave as proton donors and are important for particle charging (Zhitomirsky, 2002). A mixture of methanol and water was used as the solvent for anodic EPD of titanate nanotube in the study of Kim *et al.* (2006) and the cell provided efficiency of 6.72% which was significantly higher than the cell with titanate nanotube prepared from doctor blading method. Except from the proton

donor role of solvents, Zhitomirsky (2002) reported that non-aqueous solvent or mixture solvent with low dielectric constant could result in reducing of double layer thickness of colloid particles, which led to particle coagulation while it help to reduce the solubility of deposits. As a result, optimization for a system is needed.

Zhitomirsky (2002) found that particle charging was achieved via adsorption of protons which were formed by the keto-enol reaction catalyzed by iodine and water and the relatively stable suspensions could be obtained in isopropyl alcohol solvent instead of acetone solvent. Grinis *et al.* (2008) also found that addition of acetylacetone in particle suspension before charging the system effectively lowered the particle aggregation. Moreover, ethanol as media solvent gave the best result among methanol and isopropanol since it provided strong adherent, uniform, and homogeneous film with controllable thickness.

Other parameters control both quantity and quality of deposited film. For instance, to obtain thicker film, higher concentration of suspension, higher electric field, and longer deposition time are used. However, these are usually limited by film quality. Grinis *et al.* (2008) found that low P25 concentration gave the best DSC efficiency since high P25 content made more agglomeration and led to poor packing density. Meanwhile, Chen *et al.* (2011) explained that the morphology of the film surface could be controlled by the potential different between two electrodes because higher electric field provided less order structure and packing density, which led to non-smooth film.

Besides, the deposition temperature influences directly to the electronic property of the film. Tirosh *et al.* (2006) found that low temperature of EPD induced the preferential orientation of TiO_2 nanocrystals. This led to increase in electron transport in porous TiO_2 which reached the optimum value at 0 °C of EPD, but not influenced to the recombination rate of injected electron and electrolyte.

Nevertheless, electrodeposited films with free binder still face crack problem when deposition time is too long at an electric field. To solve this, multilayer-deposition is required (Grinis *et al.*, 2008; Chiu et al., 2011).